



## Research



**Cite this article:** Davies B, Morini L. 2024 Super band gaps and periodic approximants of generalised Fibonacci tilings. *Proc. R. Soc. A* **480**: 20230663.

<https://doi.org/10.1098/rspa.2023.0663>

Received: 10 September 2023

Accepted: 5 February 2024

**Subject Areas:**

applied mathematics, wave motion

**Keywords:**

metamaterial, quasicrystal, supercell, transmission spectra, phononic crystal, transfer matrix

**Author for correspondence:**

Bryn Davies

e-mail: [bryn.davies@imperial.ac.uk](mailto:bryn.davies@imperial.ac.uk)

# Super band gaps and periodic approximants of generalised Fibonacci tilings

Bryn Davies<sup>1</sup> and Lorenzo Morini<sup>2</sup>

<sup>1</sup>Department of Mathematics, Imperial College London, London SW7 2AZ, UK

<sup>2</sup>School of Engineering, Cardiff University, Cardiff CF24 3AA, UK

BD, 0000-0001-8108-2316; LM, 0000-0002-4574-0905

We present mathematical theory for self-similarity induced spectral gaps in the spectra of systems generated by generalised Fibonacci tilings. Our results characterise super band gaps, which are spectral gaps that exist for all sufficiently large periodic systems in a Fibonacci-generated sequence. We characterise super band gaps in terms of a growth condition on the traces of the associated transfer matrices. Our theory includes a large family of generalised Fibonacci tilings, including both precious mean and metal mean patterns. We apply our analytic results to characterise spectra in three different settings: compressional waves in a discrete mass-spring system, axial waves in structured rods and flexural waves in multi-supported beams. The theory is shown to give accurate predictions of the super band gaps, with minimal computational cost and significantly greater precision than previous estimates. It also provides a mathematical foundation for using periodic approximants (supercells) to predict the transmission gaps of quasicrystalline samples, as we verify numerically.

## 1. Introduction

Heterogeneous materials have the ability to manipulate and guide waves in carefully controlled ways. The discovery of exotic phenomena, such as negative refraction and cloaking effects, led to the name *metamaterials* being coined [1]. While many metamaterials are based on periodic arrangements of meta-atoms,

© 2024 The Authors. Published by the Royal Society under the terms of the Creative Commons Attribution License <http://creativecommons.org/licenses/by/4.0/>, which permits unrestricted use, provided the original author and source are credited.

quasi-periodic metamaterials have fascinating wave scattering and transmission properties and have the potential to greatly enlarge the metamaterial design space. However, the lack of concise mathematical methods able to describe the transmission spectra of quasi-periodic materials efficiently and with minimal computational cost, particularly at non-zero frequencies, is a significant barrier to widespread usage. In this work, we help to overcome this barrier for the specific example of quasicrystals based on Fibonacci tilings by developing the mathematical theory that establishes a simple approach for characterizing the spectral gaps.

Characterizing the spectra of quasi-periodic differential operators is a longstanding and fascinating problem [2,3]. In particular, one-dimensional Schrödinger operators with quasi-periodic potentials have been widely studied. Typical results concern the Cantor-type properties of the spectrum [4–7] and the extent to which its spectrum can be decomposed into pure-point, singularly continuous and absolutely continuous eigenvalues [8,9].

In the present work, the aim is to quantify specific spectral features, rather than characterise overall properties of the spectrum. A promising avenue in this direction, which we will not make use of in this work, is to exploit the fact that quasicrystals can be obtained through incommensurate projections of periodic patterns in higher dimensional spaces. This approach has been used to develop homogenisation methodologies [10,11], to model wave propagation in one-dimensional quasicrystals [12] and make predictions on the locations of spectral gaps [13]. In the latter case, this approach has suffered from the occurrence of spurious modes and a precise convergence theory has yet to be established. Given these challenges concerning the spectra of quasicrystals, a common strategy is to consider periodic approximants of the material, sometimes known as *supercells*. This approach is commonplace in the physical literature (for example, in [14–16]) and has the significant advantage that the spectra of the periodic approximants can be computed efficiently using Floquet–Bloch analysis. This method characterises the spectrum as a countable collection of spectral bands with *band gaps* between each band.

This work will consider the specific example of generalised Fibonacci tilings, which are a type of one-dimensional quasi-periodic patterns that can be generated by substitution rules. These patterns were classified in [17] and are formed by tiling two distinct elements, labelled  $A$  and  $B$ , according to some substitution rule

$$A \rightarrow \mathcal{M}_{ml}(A, B) \quad \text{and} \quad B \rightarrow \mathcal{M}_{m'l'}(A, B), \quad (1.1)$$

where  $\mathcal{M}_{ml}(A, B)$  is some pattern that contains the  $A$  elements  $m$  times and the  $B$  elements  $l$  times. The most widely studied example of such a tiling is the golden mean Fibonacci tiling, which is given by (1.1) with  $m = l = m' = 1$  and  $l' = 0$ . The first few terms of this sequence are shown in figure 1, from which it is clear that the sequence has the property that each word is given by combining the previous two. That is,  $\mathcal{F}_{n+1} = \mathcal{F}_n \cup \mathcal{F}_{n-1}$ , which is an equivalent definition for the golden mean Fibonacci tiling. Generalised Fibonacci tilings have been studied extensively in the literature for various elastic, mechanical and Hamiltonian systems [18–24]. Complex patterns of stop and pass bands have been observed, whose features include large stop bands across multiple frequency scales and self-similar properties.

In the setting of tilings where the quasi-crystalline pattern is generated using a substitution rule, giving a growing sequence of tilings, the use of periodic approximants is particularly promising. A natural question to ask is how the band gaps evolve as the unit cell is grown according to the given tiling rule. An example is shown in figure 2, where we plot the band diagrams for a system of axial waves in structured rods (which will be examined in detail in §4b) with the unit cell designed to follow the golden mean Fibonacci tiling. We can see that while the Bloch spectrum of the Fibonacci tilings  $\mathcal{F}_n$  becomes increasingly complex as  $n$  grows, there are some clear features that emerge. As  $n$  increases, the pattern of pass bands and band gaps becomes increasingly fragmented, reminiscent of the Cantor-type behaviour predicted by the literature for other quasi-periodic operators [4–7]. In spite of this complexity, several large band gaps seem to appear for relatively small  $n$  (e.g. for  $\mathcal{F}_4$ ) and persist as  $n$  grows. These features were noted in [23], who coined the phrase *super band gaps* to describe these features.



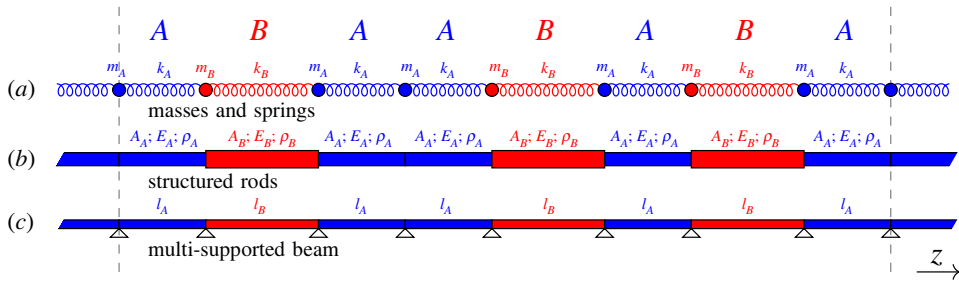


**Figure 3.** One-dimensional wave systems with periodic unit cells corresponding to the golden mean Fibonacci tiling  $\mathcal{F}_5 = ABAABABA$  are shown. (a) A discrete system of masses coupled with springs, where we modulate both the masses  $m_X$  and the spring constants  $k_X$ . (b) Axial waves in structured rods, where the cross sections  $A_X$ , Young's modulus  $E_X$  and the mass density  $\rho_X$  can be modulated. (c) Flexural waves in multi-supported beams, where the distances  $l_X$  between the supports are varied.

and mass density). Finally, we will consider a continuous flexural beam that is supported at varying intervals. We will examine these three systems in detail in §4 and present numerical results showing that our theory for super band gaps can be used to reveal spectral features accurately and with minimal computational cost.

## 2. Generalised Fibonacci tilings

Generalised Fibonacci structures are defined according to the substitution rule

$$A \rightarrow A^m B^l, \quad B \rightarrow A, \quad (2.1)$$

where  $m$  and  $l$  are positive integers. Typically, the sequence is initiated with  $\mathcal{F}_0 = B$ , which yields that  $\mathcal{F}_1 = A$ ,  $\mathcal{F}_2 = A^m B^l$ ,  $\mathcal{F}_3 = (A^m B^l)^m A^l$  and so on (figure 1). This sequence has the property that each word is the combination of  $m$  and  $l$  versions of the previous two

$$\mathcal{F}_{n+1} = \underbrace{\mathcal{F}_n \cup \dots \cup \mathcal{F}_n}_{m \text{ times}} \cup \underbrace{\mathcal{F}_{n-1} \cup \dots \cup \mathcal{F}_{n-1}}_{l \text{ times}}. \quad (2.2)$$

Examples of periodic mass-spring systems with unit cells given by the golden mean Fibonacci tilings ( $m = l = 1$ )  $\mathcal{F}_2, \mathcal{F}_3, \mathcal{F}_4$  and  $\mathcal{F}_5$  are depicted in figure 4. The total number of elements in  $\mathcal{F}_n$  is given by the  $n$ th generalised Fibonacci number  $F_n$ , which are defined according to the recurrence relation

$$F_n = mF_{n-1} + lF_{n-2}. \quad (2.3)$$

The limit of the ratio  $F_{n+1}/F_n$  as  $n \rightarrow \infty$  is given by

$$\sigma(m, l) := \lim_{n \rightarrow \infty} \frac{F_{n+1}}{F_n} = \frac{m + \sqrt{m^2 + 4l}}{2}, \quad (2.4)$$

and the tilings inherit their names from this limiting ratio. For example, since  $\sigma(1, 1) = (1 + \sqrt{5})/2 \approx 1.618 \dots$ , this case is often known as the golden mean Fibonacci tiling. Similarly,  $\sigma(2, 1) = 1 + \sqrt{2} \approx 2.414 \dots$  is the silver mean and  $\sigma(3, 1) = (3 + \sqrt{13})/2 \approx 3.303 \dots$  is the bronze mean. Likewise,  $\sigma(1, 2)$  and  $\sigma(1, 3)$  have assumed the names copper mean and nickel mean, respectively.

We will study wave propagation in systems that have two degrees of freedom, in the sense that their behaviour can be described fully by a two-element state vector  $\mathbf{u}_j \in \mathbb{R}^2$ , where  $j$  is an index denoting the spatial position. We suppose that wave propagation in these systems can be described by a unimodular transfer matrix  $T(\omega)$  with real-valued entries. That is, for any indices  $i$  and  $j$  and any frequency  $\omega$ , there is some matrix  $T(\omega) \in \mathbb{R}^{2 \times 2}$  such that  $\det(T) = 1$  and  $\mathbf{u}_i = T(\omega)\mathbf{u}_j$ . We will explore three different examples of such systems in §4.

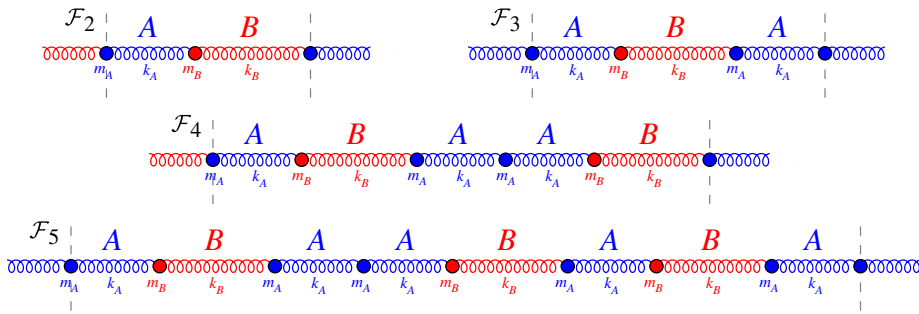


**Figure 4.** Periodic mass-spring systems with unit cells given by the golden mean Fibonacci tilings  $\mathcal{F}_2$  to  $\mathcal{F}_5$ . Both the masses and the spring constants can be modulated between the two phases (labelled  $A$  and  $B$ ).

We let  $T_n$  be the transfer matrix associated with the structure  $\mathcal{F}_n$ . As a result of the property (2.2), the substitution rule (2.1) means that this sequence of transfer matrices satisfies

$$T_{n+1} = T_{n-1}^l T_n^m. \quad (2.5)$$

We are interested in studying structures formed by repeating  $\mathcal{F}_n$  periodically. We can relate the state vector at either ends of the unit cell  $\mathcal{F}_n$  by

$$\mathbf{u}_{F_n} = T_n(\omega)\mathbf{u}_0. \quad (2.6)$$

Then, to understand the transmission properties of the periodic material, we can apply the Floquet–Bloch theorem. If  $L_n$  is the length of the unit cell  $\mathcal{F}_n$ , then we substitute  $\mathbf{u}_{F_n} = \mathbf{u}_0 e^{iKL_n}$  into equation (2.6), giving that  $\det(T_n(\omega) - e^{iKL_n}I) = 0$ . Using the fact that  $\det(T_n) = 1$ , this reduces to the simple dispersion relation

$$\cos(KL_n) = \frac{1}{2} \text{tr}(T_n(\omega)). \quad (2.7)$$

This has a real solution for  $K$  if and only if  $|\text{tr}(T_n(\omega))| \leq 2$ . If  $\omega$  is such that  $K$  is complex, then we do not have Floquet–Bloch modes so  $\omega$  is said to lie in a *band gap* of the periodic material. Examples of the dispersion diagrams obtained by solving (2.7) for periodic materials with unit cells given by the Fibonacci tilings  $\mathcal{F}_2$  and  $\mathcal{F}_5$  are shown on the left in figure 2. This is for the case of axial waves in structured rods, which will be studied in detail in §4b. The shaded regions that lie between the dispersion curves are the band gaps. On the right in figure 2, we show the band gaps (without the associated dispersion curves) for the first 10 Fibonacci tilings  $\mathcal{F}_1$  to  $\mathcal{F}_{10}$ .

Characterizing the band gaps of the material reduces to finding  $\omega$  such that  $|\text{tr}(T_n(\omega))| > 2$ . Given the importance of the transfer matrix trace, we define the quantity

$$x_n(\omega) = \text{tr}(T_n(\omega)). \quad (2.8)$$

Understanding how the sequence  $\{x_n(\omega) : n = 0, 1, 2, \dots\}$  evolves for different materials and at different frequencies  $\omega$  will be the main theoretical challenge tackled in this work. In particular, we will define a super band gap to be the set  $\mathcal{S}_N$  of all  $\omega \in \mathbb{R}$  which are in band gaps of  $\mathcal{F}_n$  for all  $n \geq N$ :

**Definition 2.1.** Given a sequence of periodic materials indexed by  $n = 0, 1, 2, \dots$  which have associated transfer matrices  $T_n(\omega) \in \mathbb{R}^{2 \times 2}$ , a *super band gap*  $\mathcal{S}_N \subset \mathbb{R}$  is defined as

$$\mathcal{S}_N := \{\omega \in \mathbb{R} : |\text{tr}(T_n(\omega))| > 2 \text{ for all } n \geq N\}.$$

In this work, we will characterise super band gaps in Fibonacci tiling by deriving ‘growth conditions’ that guarantee a frequency being in a super band gap. These results say that if  $\omega$  is such that there exists some  $N \in \mathbb{N}$  for which  $|x_N(\omega)| > 2$  and the following terms  $|x_{N+1}(\omega)|$  and  $|x_{N+2}(\omega)|$  grow sufficiently quickly (in a sense that will depend on the choice of tiling parameters

$l$  and  $m$ ), then  $\omega$  is guaranteed to be in the super band gap  $S_N$ . This analysis will rest upon the helpful observation that the traces corresponding to generalised Fibonacci tilings satisfy recursive relations [25,26]. To state these recursion relations, we must first introduce the quantity

$$t_n(\omega) := \text{tr}(T_{n-2}(\omega)T_{n-1}(\omega)). \quad (2.9)$$

We will also need the sequence of polynomials  $d_k(x)$ , defined recursively by

$$d_0(x) = 0, \quad d_1(x) = 1 \quad \text{and} \quad d_k(x) = xd_{k-1}(x) - d_{k-2}(x) \quad \text{for } k \geq 2. \quad (2.10)$$

We have that  $d_2(x) = x$ ,  $d_3(x) = x^2 - 1$ ,  $d_4(x) = x^3 - 2x$ ,  $d_5(x) = x^4 - 3x^2 + 1$  and so on. These polynomials are rescaled Chebyshev polynomials of the second kind. Understanding the properties of these polynomials (in §3c) will be one of the key insights that will allow us to prove spectral properties of generalised Fibonacci tilings for large values of  $m$  or  $l$ . Finally, we have the following recursion relation describing the evolution of  $x_n$  and  $t_n$ , which was shown in [27]

$$\text{and} \quad \left. \begin{aligned} x_{n+1} &= d_m(x_n)[d_l(x_{n-1})t_{n+1} - d_{l-1}(x_{n-1})x_n] \\ &\quad - d_{m-1}(x_n)[d_{l+1}(x_{n-1}) - d_{l-1}(x_{n-1})] \\ t_{n+1} &= d_{m+1}(x_{n-1})[d_l(x_{n-2})t_n - d_{l-1}(x_{n-2})x_{n-1}] \\ &\quad - d_m(x_{n-1})[d_{l+1}(x_{n-2}) - d_{l-1}(x_{n-2})]. \end{aligned} \right\} \quad (2.11)$$

The name ‘super band gap’ was introduced in [23], who observed their existence in generalised Fibonacci structures (corresponding to the golden and silver means). They succeed in predicting the approximate locations of these super band gaps using the function  $H_n : \mathbb{R} \rightarrow [0, \infty)$  defined by

$$H_n(\omega) = |\text{tr}(T_n(\omega))\text{tr}(T_{n+1}(\omega))|. \quad (2.12)$$

They observed numerically that if  $\omega \in \mathbb{R}$  is such that  $H_2(\omega) \gg 2$ , then it is likely to be in a super band gap. Other approximate approaches for predicting the locations of super band gaps also exist, such as considering an ‘effective lattice’ that is the superposition of two periodic lattices, with periods differing by a ratio equal to the golden mean [16]. This work builds on these previous results by developing the first rigorous justification for the occurrence of super band gaps in materials generated by generalised Fibonacci tilings.

### 3. Theory of super band gaps

In this section, we will develop the main theory characterizing super band gaps in materials generated by generalised Fibonacci tilings. These results will take the form of growth conditions, which will need to be modified to suit different values of  $m$  and  $l$ . We will apply this theory to specific physical examples in §4 and use it to predict the transmission coefficient of large but finite-sized samples in §5.

#### (a) Golden mean Fibonacci

This is the classical Fibonacci tiling, where  $m = 1$  and  $l = 1$  in (2.1). It is referred to as the *golden mean* Fibonacci tiling because the limiting ratio is  $\sigma(1, 1) = (1 + \sqrt{5})/2 \approx 1.618$ , the famous golden mean that appears in nature. In the golden mean Fibonacci tiling, the recursion relation (2.11) can be simplified to a much simpler form, given by

$$x_{n+1} = x_n x_{n-1} - x_{n-2}, \quad n \geq 2. \quad (3.1)$$

This was discovered in [28] and has been the basis of many subsequent studies of Fibonacci materials.

The main result we will use to characterise super band gaps is the following theorem. This shows that if a frequency is such that the sequence of traces is outside of  $[-2, 2]$  and has three subsequent terms that are growing, then that frequency is in a super band gap of the golden mean Fibonacci tiling. This result is a modification of the lemma 3.3 in [29], where it was proved for the

special case where successive terms are double the previous term (giving exponential growth of the sequence). Here, we have improved the tightness of the bound and shown that any growth rate bigger than 1 is sufficient for a super band gap to exist.

**Theorem 3.1.** *Let  $\omega \in \mathbb{R}$  and consider  $x_n(\omega)$  satisfying the golden mean recursion relation (3.1). Suppose that there exists some  $N \in \mathbb{N}$  such that*

$$|x_N| > 2, |x_{N+1}| \geq |x_N| \quad \text{and} \quad |x_{N+2}| \geq |x_{N+1}|.$$

*Then  $|x_{n+1}| \geq |x_n|$  for all  $n > N$ . Consequently,  $|x_n| > 2$  for all  $n \geq N$ , meaning that  $\omega$  is in the super band gap  $\mathcal{S}_N$ .*

*Proof.* We will show that  $|x_{N+3}| \geq |x_{N+2}|$ , from which the result will follow by induction. We have that

$$|x_{N+3}| \geq |x_{N+2}||x_{N+1}| - |x_N| \geq |x_{N+2}||x_N| - |x_N| = |x_{N+2}|(|x_N| - 1) + (|x_{N+2}| - |x_N|). \quad (3.2)$$

By hypothesis, we have that  $|x_N| - 1 > 1$  and  $|x_{N+2}| \geq |x_N|$ , so it holds that  $|x_{N+3}| \geq |x_{N+2}|$ . ■

## (b) Silver mean Fibonacci

The case where  $m = 2$  and  $l = 1$  in (2.1) is known as the *silver mean* Fibonacci, again inheriting its name from the limit  $\sigma(2, 1) = 1 + \sqrt{2} \approx 2.414$ . After some rearrangement, the corresponding recursion rule is given by

$$\left. \begin{aligned} x_{n+1} &= x_n t_{n+1} - x_{n-1} \\ t_{n+1} &= x_n x_{n-1} - t_n \end{aligned} \right\} \quad (3.3)$$

and

for  $n \geq 2$ . While this is more complicated than in the case of the golden mean, it turns out that super band gaps can be characterised using the same condition (although the proof of this is slightly less straightforward than the single-line argument of theorem 3.1).

**Theorem 3.2.** *Let  $\omega \in \mathbb{R}$  and consider  $x_n(\omega)$  satisfying the silver mean recursion relation (3.3). Suppose that there exists some  $N \in \mathbb{N}$  such that*

$$|x_N| > 2, |x_{N+1}| \geq |x_N| \quad \text{and} \quad |x_{N+2}| \geq |x_{N+1}|.$$

*Then  $|x_{n+1}| \geq |x_n|$  for all  $n > N$ . Consequently,  $|x_n| > 2$  for all  $n \geq N$ , meaning that  $\omega$  is in the super band gap  $\mathcal{S}_N$ .*

*Proof.* As for the golden mean Fibonacci tiling, the strategy will be to proceed by induction. We begin with the second equation of the recursion relation (3.3), with a view to deriving a lower bound on  $|t_{N+3}|$ . Observe, first, that thanks to elementary properties of unimodular matrices

$$t_n = \text{tr}(T_{n-2}T_{n-1}) \leq \frac{1}{2}(\text{tr}(T_{n-2}^2) + \text{tr}(T_{n-1}^2)) = \frac{1}{2}(x_{n-2}^2 + x_{n-1}^2) - 2, \quad (3.4)$$

for any  $n$ . In particular, since  $|x_N| > 2$  and  $|x_{N+1}| > 2$ , the right-hand side of (3.4) is positive when  $n = N + 2$ , so we have that

$$|t_{N+2}| \leq \frac{1}{2}(x_N^2 + x_{N+1}^2) - 2 \leq x_{N+1}^2 - 2. \quad (3.5)$$

Then, the second equation of (3.3) gives

$$|t_{N+3}| \geq |x_{N+2}||x_{N+1}| - |t_{N+2}| \geq x_{N+1}^2 - x_{N+1}^2 + 2 = 2. \quad (3.6)$$

Finally, turning to the first equation of (3.3), we see that

$$|x_{N+3}| \geq |x_{N+2}||t_{N+3}| - |x_{N+1}| \geq 2|x_{N+2}| - |x_{N+1}| \geq |x_{N+2}|. \quad (3.7)$$

Then, by induction, it follows that  $|x_{n+1}| \geq |x_n|$  for all  $n > N$ . ■

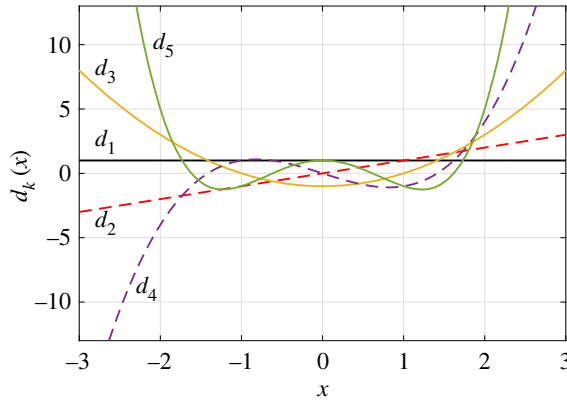


**Figure 5.** The first few Chebyshev polynomials  $d_k(x)$ , defined recursively in (2.10). These functions play a crucial role in determining the behaviour of generalised Fibonacci tilings.

### (c) Properties of the Chebyshev polynomials

Before proceeding to study super band gaps in more exotic generalised Fibonacci tilings, we must first prove some properties of the polynomials  $d_k(x)$  defined in (2.10). The first few  $d_k(x)$  are plotted in figure 5, for reference. Using standard techniques (as in e.g. §2.3 of [30]), we can derive an explicit formula for  $d_k(x)$ , which is given by

$$d_k(x) = \frac{1}{\sqrt{x^2 - 4}} \left( \frac{x + \sqrt{x^2 - 4}}{2} \right)^k - \frac{1}{\sqrt{x^2 - 4}} \left( \frac{x - \sqrt{x^2 - 4}}{2} \right)^k, \quad (3.8)$$

for  $k \in \mathbb{Z}^{\geq 0}$  and  $x \in (0, \infty) \setminus \{2\}$ . To check the value of the solution at  $x = 2$ , we have the following lemma:

**Lemma 3.3.**  $d_k(2) = k$  for all  $k \geq 0$ .

*Proof.* This is true, by definition, for  $k = 0$  and  $k = 1$ . If we suppose that it holds for arbitrary  $k - 1$  and  $k$  then we have that

$$d_{k+1}(2) = 2d_k(2) - d_{k-1}(2) = 2k - (k - 1) = k + 1, \quad (3.9)$$

so the result follows by induction on  $k$ . ■

The definition 2.10, alongside the formula (3.8), can be used to study the properties of the sequence of polynomials. For example, it will be helpful to understand the parity of  $d_k$ .

**Lemma 3.4.** For  $k \geq 1$ , if  $k$  is even then  $d_k(x)$  contains only odd powers of  $x$ , whereas if  $k$  is odd then  $d_k(x)$  contains only even powers of  $x$ .

*Proof.* We can immediately check the first few terms:  $d_1(x) = 1$ ,  $d_2(x) = x$ ,  $d_3(x) = x^2 - 1$ . Then, we suppose that the statement holds true for some  $k$  and  $k - 1$ , where  $k$  is even. In which case  $xd_k(x)$  contains only odd powers of  $x$ , meaning that  $d_{k+1}(x) = xd_k(x) - d_{k-1}(x)$  contains only odd powers. A similar argument holds for odd  $k$ . The result follows by induction. ■

A consequence of lemma 3.4 is that  $d_k$  is an even function when  $k$  is odd and is an odd function when  $k$  is even. This means it is sufficient to study its properties when  $x > 0$ . We have the following results, which will allow us to derive bounds on these polynomials when  $|x| > 2$  (which is the domain of interest).

**Lemma 3.5.**  $d_k(x) \geq 0$  and  $d'_k(x) \geq 0$  for all  $k \geq 0$  and all  $x \geq 2$ , with equality holding only if  $k = 0$ .

*Proof.* This is trivial for  $k=0$ , so we consider  $k \geq 1$ . From lemma 3.3, we have that  $d_k(2) = k > 0$  for all  $k \geq 1$ . For  $x > 2$ , it holds that  $x + \sqrt{x^2 - 4} > x - \sqrt{x^2 - 4} > 0$ . Thus, since  $x \mapsto x^k$  is strictly increasing for  $x \geq 0$ , it follows that

$$\left(x + \sqrt{x^2 - 4}\right)^k - \left(x - \sqrt{x^2 - 4}\right)^k > 0. \quad (3.10)$$

So, using the formula (3.8), we find that  $d_k(x) > 0$  for  $k \geq 1$  and  $x > 2$ .

To handle the derivative, we note that  $d_k(x)$  is the determinant of the  $k \times k$  tridiagonal matrix  $M_k(x)$  given by

$$M_k(x)_{ij} = \begin{cases} x & \text{if } i = j, \\ 1 & \text{if } i - j = \pm 1, \\ 0 & \text{otherwise.} \end{cases} \quad (3.11)$$

Since  $d_k(x) > 0$  for  $k \geq 1$  and  $x \geq 2$ ,  $M_k(x)$  must be invertible. Hence, we can use Jacobi's formula to see that

$$\frac{d}{dx} d_k(x) = \frac{d}{dx} \det(M_k(x)) = \det(M_k(x)) \operatorname{tr} \left( M_k(x)^{-1} \frac{d}{dx} M_k(x) \right) = d_k(x) \operatorname{tr}(M_k(x)^{-1}), \quad (3.12)$$

where we have used the fact that the derivative of  $M_k(x)$  with respect to  $x$  is the identity matrix.

To deal with  $\operatorname{tr}(M_k(x)^{-1})$ , we will show that  $M_k(x)$  has strictly positive eigenvalues whenever  $k \geq 1$  and  $x \geq 2$ . For  $x > 2$ , this follows immediately from the Gershgorin circle theorem [31, Theorem 6.1.1]. When  $x = 2$ , Gershgorin circle theorem permits eigenvalues to vanish, but this is forbidden by the invertibility of  $M_k(x)$ . Thus, if  $k \geq 1$  and  $x \geq 2$ , then  $M_k(x)$  has strictly positive eigenvalues  $\lambda_1(x), \dots, \lambda_k(x)$ . Finally, using the fact that  $M_k(x)$  is symmetric and positive definite, we can compute that

$$\operatorname{tr}(M_k(x)^{-1}) = \sum_{i=1}^k \lambda_i(x)^{-1} > 0. \quad (3.13)$$

Combining this with the fact that  $d_k(x) > 0$ , (3.12) tells us that  $d'_k(x) > 0$  for all  $k \geq 1$  and  $x \geq 2$ . ■

**Corollary 3.6.**  $|d_k(x)| \geq 2$  for all  $k \geq 2$  and all  $|x| \geq 2$ .

*Proof.* This follows by combining lemma 3.5 with lemma 3.3, for  $x > 2$ . Then, the result for  $x < -2$  follows by parity. ■

**Lemma 3.7.**  $d_{k+1}(x) \geq d_k(x)$  for all  $k \geq 0$  and all  $x \geq 2$ .

*Proof.* This is true for  $k = 0$ , from the definition. Then, supposing that  $d_k(x) \geq d_{k-1}(x)$ ,

$$d_{k+1}(x) = xd_k(x) - d_{k-1}(x) \geq 2d_k(x) - d_{k-1}(x) = d_k(x) + (d_k(x) - d_{k-1}(x)) \geq d_k(x), \quad (3.14)$$

where the first inequality relies on the fact that  $d_k(x) \geq 0$  from lemma 3.5. Finally, the result follows by induction on  $k$ . ■

Using the odd/even parity of the polynomials  $d_k$ , we have the following corollary:

**Corollary 3.8.**  $|d_{k+1}(x)| \geq |d_k(x)|$  for all  $k \geq 0$  and all  $|x| \geq 2$ .

The final property of the polynomials  $d_k(x)$  that we will need is the following inequality:

**Lemma 3.9.**  $|d_{k+1}(x)| \leq |xd_k(x)| \leq 2|d_{k+1}(x)|$  for any  $|x| > 2$  and any  $k \geq 1$ .

*Proof.* Thanks to the parity of  $d_k$ , we can consider  $x > 2$  without loss of generality, in which case  $d_k(x) \geq 0$  for all  $k$ . For the first inequality, we have that

$$0 \leq d_{k-1}(x) = xd_k(x) - d_{k+1}(x), \quad (3.15)$$

so  $d_{k+1}(x) \leq xd_k(x)$ . To see the second inequality, we must use the formula (3.8). It holds that

$$d_{k+1}(x) = \frac{1}{\sqrt{x^2-4}} \frac{x + \sqrt{x^2-4}}{2} \left( \frac{x + \sqrt{x^2-4}}{2} \right)^k - \frac{1}{\sqrt{x^2-4}} \frac{x - \sqrt{x^2-4}}{2} \left( \frac{x - \sqrt{x^2-4}}{2} \right)^k. \quad (3.16)$$

We have that  $x + \sqrt{x^2-4} \geq x$  and  $-(x - \sqrt{x^2-4}) \geq -x$ , from which we see that  $d_{k+1}(x) \geq (1/2)xd_k(x)$ . ■

### (d) Generalised precious mean Fibonacci

Generalised Fibonacci tilings with  $l=1$  and arbitrary  $m$  are known as *precious mean* Fibonacci tilings (generalizing the notions of golden and silver means for  $m=1$  and  $m=2$ , respectively). In this case, the recursion relation (2.11) reads

$$\left. \begin{aligned} x_{n+1} &= d_m(x_n)t_{n+1} - d_{m-1}(x_n)x_{n-1} \\ \text{and} \quad t_{n+1} &= d_{m+1}(x_{n-1})t_n - d_m(x_{n-1})x_{n-2} \end{aligned} \right\} \quad (3.17)$$

for  $n \geq 2$ . In order to develop a precise theory for super band gaps when  $m > 2$ , we will need to assume that the sequence of traces has at least polynomial growth, with order  $m-1$ . This is consistent with the rule that was established for the silver mean in theorem 3.2. In fact, we will need that terms grow such that  $|x_{n+1}| \geq |d_{m-1}(x_n)x_n|$ . This is made precise by the following theorem.

**Theorem 3.10.** *Let  $\omega \in \mathbb{R}$  and consider  $x_n(\omega)$  satisfying the generalised precious mean recursion relation (3.17) for some  $m \geq 2$ . Suppose that there exists some  $N \in \mathbb{N}$  such that*

$$|x_N| > 2, \quad |x_{N+1}| \geq |d_{m-1}(x_N)x_N| \quad \text{and} \quad |x_{N+2}| \geq |d_{m-1}(x_{N+1})x_{N+1}|.$$

*Then  $|x_{n+1}| \geq |d_{m-1}(x_n)x_n|$  for all  $n > N$ . Consequently,  $|x_n| > 2$  for all  $n \geq N$ , meaning that  $\omega$  is in the super band gap  $\mathcal{S}_N$ .*

*Proof.* The special case  $m=2$  is exactly the result that was proved in theorem 3.2, since  $d_1(x) = 1$ . We will consider  $m \geq 3$ . We begin by rewriting the recursion relation (3.17) in this case. From the first equation of (3.17), we have that

$$d_m(x_{n-1})t_n = x_n + d_{m-1}(x_{n-1})x_{n-2}. \quad (3.18)$$

Turning to the second equation of (3.17), using the definition of  $d_k$  and substituting (3.18) gives

$$t_{n+1} = x_{n-1}x_n + d_{m-2}(x_{n-1})x_{n-2} - d_{m-1}(x_{n-1})t_n. \quad (3.19)$$

An important observation is that, thanks to corollary 3.6, the hypotheses of this theorem imply that  $|x_{N+2}| \geq |x_{N+1}| \geq |x_N| > 2$ . This is important as  $\omega$  could not be in the super band gap  $\mathcal{S}_N$  otherwise. It also allows us to use the inequality (3.4) to see that

$$|t_{N+2}| \leq x_{N+1}^2 - 2. \quad (3.20)$$

Then, from (3.19), we have that

$$\begin{aligned} |t_{N+3}| &\geq |x_{N+1}x_{N+2}| - |d_{m-2}(x_{N+1})x_N| - |d_{m-1}(x_{N+1})t_{N+2}| \\ &\geq |x_{N+1}x_{N+2}| - |d_{m-2}(x_{N+1})x_N| + 2|d_{m-1}(x_{N+1})| - |x_{N+1}^2 d_{m-1}(x_{N+1})| \\ &\geq -|d_{m-2}(x_{N+1})x_N| + 2|d_{m-1}(x_{N+1})|, \end{aligned} \quad (3.21)$$

where the last inequality follows by hypothesis.

To deal with (3.21), we must turn to lemma 3.9. Since  $|x_N| > 2$ ,  $|d_{m-1}(x_N)| \geq |d_2(x_N)| \geq d_2(2) = 2$ . As a result, the assumption that  $|x_{N+1}| \geq |x_N d_{m-1}(x_N)|$  implies that  $|x_{N+1}| \geq 2|x_N| > 4$ . Consequently, we have that

$$|d_{m-2}(x_{N+1})x_N| \leq \frac{1}{2}|d_{m-2}(x_{N+1})x_{N+1}| \leq |d_{m-1}(x_{N+1})|. \quad (3.22)$$

Using this inequality, (3.21) gives us that

$$|t_{N+3}| \geq |d_{m-1}(x_{N+1})| \geq d_2(4) = 4. \quad (3.23)$$

We can now turn to the first equation of (3.17), which gives us that

$$|x_{N+3}| \geq |d_m(x_{N+2})t_{N+3}| - |d_{m-1}(x_{N+2})x_{N+1}| \geq 4|d_m(x_{N+2})| - |d_{m-1}(x_{N+2})x_{N+1}|. \quad (3.24)$$

Using lemma 3.9 again, we have that

$$|x_{N+3}| \geq 2|d_{m-1}(x_{N+2})x_{N+2}| - |d_{m-1}(x_{N+2})x_{N+1}| \geq |d_{m-1}(x_{N+2})x_{N+2}|, \quad (3.25)$$

where the second inequality follows from the fact that  $|x_{N+2}| \geq |x_{N+1}|$ . Proceeding by induction gives us that  $|x_{n+1}| \geq |d_{m-1}(x_n)x_n|$  for all  $n > N$ . Thanks to corollary 3.6, we see also that  $|x_n| \geq |x_N| > 2$  for all  $n \geq N$ . ■

### (e) Generalised metal mean Fibonacci

Suppose now that  $m = 1$  and  $l$  is arbitrary. This case is sometimes known as the *metal mean* generalised Fibonacci. In particular,  $l = 2$  is known as the *copper mean* and  $l = 3$  as the *nickel mean* [6,32]. In this case, we are able to eliminate  $t_n$  from the recursion relation (2.11), giving the simpler recursion relation

$$x_{n+1} = d_l(x_{n-1})[x_n x_{n-1} - d_{l+1}(x_{n-2}) + d_{l-1}(x_{n-2})] - x_n d_{l-1}(x_{n-1}) \quad (3.26)$$

for  $n \geq 2$ . Note how this reduces to the golden mean recursion relation (3.1) in the case that  $l = 1$ .

**Theorem 3.11.** *Let  $\omega \in \mathbb{R}$  and consider  $x_n(\omega)$  satisfying the generalised metal mean recursion relation (3.26) for some  $l \geq 1$ . Suppose that there exists some  $N \in \mathbb{N}$  such that*

$$|x_N| > 2, \quad |x_{N+1}| \geq \frac{5}{2} \quad \text{and} \quad |x_{N+2}| \geq \max\{|x_{N+1}|, |d_{l+1}(x_N)|\}.$$

Consequently,  $|x_n| > 2$  for all  $n \geq N$ , meaning that  $\omega$  is in the super band gap  $\mathcal{S}_N$ .

*Proof.* The special case  $l = 1$  was proved in theorem 3.1. For  $l \geq 2$ , we have from (3.26) that

$$|x_{N+3}| \geq |x_{N+1}x_{N+2}d_l(x_{N+1})| - |d_l(x_{N+1})[d_{l+1}(x_N) - d_{l-1}(x_N)]| - |x_{N+2}d_{l-1}(x_{N+1})|. \quad (3.27)$$

We know that  $|d_{l+1}(x_N)| \geq |d_{l-1}(x_N)|$  and they must both have the same sign since they have the same parity and do not vanish on  $|x_N| > 2$ . As a result, we have that

$$|d_{l+1}(x_N) - d_{l-1}(x_N)| = |d_{l+1}(x_N)| - |d_{l-1}(x_N)| \leq |d_{l+1}(x_N)| \leq |x_{N+2}|, \quad (3.28)$$

where the final inequality follows by hypothesis. Substituting this into (3.27) gives

$$\begin{aligned} |x_{N+3}| &\geq |x_{N+1}x_{N+2}d_l(x_{N+1})| - |x_{N+2}d_l(x_{N+1})| - |x_{N+2}d_{l-1}(x_{N+1})| \\ &\geq (|x_{N+1}| - 2)|x_{N+2}d_l(x_{N+1})|. \end{aligned} \quad (3.29)$$

Since  $|x_{N+1}| < |x_{N+2}|$ , we can use lemma 3.9 to see that  $|x_{N+2}d_l(x_{N+1})| \geq |x_{N+1}d_l(x_{N+1})| \geq |d_{l+1}(x_{N+1})|$ . Since  $|x_{N+1}| - 2 > 0$ , we conclude that

$$|x_{N+3}| \geq |d_{l+1}(x_{N+1})|. \quad (3.30)$$

We also need to check that  $|x_{N+3}| \geq |x_{N+2}|$ . This follows from (3.29) since  $|d_l(x_{N+1})| \geq d_l(2) = l \geq 2$  and  $|x_{N+1}| - 2 \geq 1/2$ .

Finally, we can proceed by induction to see that  $|x_{n+2}| \geq \max\{|x_{n+1}|, |d_{l+1}(x_n)|\}$  for all  $n \geq N$ . Since  $|x_{n+1}| \geq 5/2$  for all  $n \geq N$ , it follows that  $|x_n| > 2$  for all, so it must hold that  $\omega \in \mathcal{S}_N$ . ■

## (f) Discussion

We have established a new theory for super band gaps, which characterises when the sequence of traces  $x_n(\omega)$  is guaranteed to grow indefinitely. A natural question to ask of the results proved in this section is whether the growth conditions are optimal. In the case of theorems 3.1 and 3.2, the results for the golden and silver mean tilings respectively, it is a reasonable hypothesis that the simple growth condition could be the strongest possible condition that guarantees the existence of a super band gap. However, we suspect that the growth conditions for the other generalised Fibonacci tilings are not the tightest possible growth bounds. For example, in the result for generalised metal mean Fibonacci tilings from theorem 3.11, the requirement that  $|x_{N+1}| \geq 5/2$  is almost certainly not optimal. We used this assumption to derive one of the bounds needed for the inductive hypothesis; however, it is likely that this assumption could be relaxed by future work. Nevertheless, the numerical evidence we will present in §4 suggests that even this sub-optimal result gives a precise prediction of the super band gaps (we will present numerical results for the copper mean tiling for each physical system). The reason for this is that within these super band gaps (particularly away from the edges) the sequence of traces  $x_n(\omega)$  typically grows very quickly, so the sub-optimality of the growth condition has little effect. This very rapid growth in the middle of super band gaps is also the reason that the estimator  $H_2(\omega)$ , defined in (2.12) and introduced by [23], performed relatively well at predicting their approximate locations. The present theory builds on this by developing an approach that is grounded in first-principles mathematical analysis.

## 4. Super band gaps in specific one-dimensional systems

The general theory from the previous section can be applied to study the spectral properties of generalised Fibonacci tilings in various one-dimensional systems. We will consider three different examples: a discrete mass-spring system, a structured rod and a continuous beam with modulated distances between the supports, as depicted in figure 3.

### (a) Compressional waves in discrete mass-spring systems

As a first example, we consider a periodic discrete mass-spring system. The fundamental cells are designed according to the generalised Fibonacci substitution rule (2.1), where the two elements  $A$  and  $B$  correspond to different masses  $m_A$  and  $m_B$  and linear springs with stiffness  $k_A$  and  $k_B$ , respectively (see figure 3a). In order to study the dispersive properties of harmonic compressional waves in this system, we study the horizontal displacement of each mass  $u_j(t) = u_j e^{i\omega t}$  and the harmonic force acting on that mass  $f_j(t) = f_j e^{i\omega t}$ , where the index  $j$  indicates the relevant mass. Thus, we introduce the state vector in the frequency domain  $\mathbf{u}_j = [u_j, f_j]^T$ . The relationship between  $\mathbf{u}_j$  and the state vector of the preceding element  $\mathbf{u}_{j-1}$  is given in [33]:

$$\mathbf{u}_j = \begin{bmatrix} u_j \\ f_j \end{bmatrix} = \begin{bmatrix} 1 & -\frac{1}{k_X} \\ m_X \omega^2 & 1 - \frac{m_X \omega^2}{k_X} \end{bmatrix} \begin{bmatrix} u_{j-1} \\ f_{j-1} \end{bmatrix} \equiv T^X(\omega, m_X, k_X) \mathbf{u}_{j-1}, \quad (4.1)$$

where  $X \in \{A, B\}$  and  $T^X(\omega, m_X, k_X)$  is the transfer matrix of a single element  $A$  or  $B$ , corresponding to the product of the respective transfer matrices associated with the mass  $m_X$  and the spring of stiffness  $k_X$  [34].

Given a generalised Fibonacci unit cell  $\mathcal{F}_n$ , the state vector  $\mathbf{u}_{F_n}$  at the right-hand boundary of the unit cell (corresponding to  $j = F_n$ , where  $F_n$  is the previously defined generalised Fibonacci

number) can then be expressed in terms of the state vector at the left-hand boundary,  $\mathbf{u}_0$ , according to

$$\mathbf{u}_{F_n} = T_n(\omega)\mathbf{u}_0, \quad (4.2)$$

where  $T_n(\omega) = \prod_{p=1}^{F_n} T^X(\omega, m_X, k_X)$  is the transfer matrix of the fundamental cell of order  $n$ . Applying the Floquet–Bloch theorem to the unit cell, we substitute  $\mathbf{u}_{F_n} = \mathbf{u}_0 e^{iKL_n}$  into equation (4.2), and due to the fact that  $T_n(\omega)$  is endowed with the unimodularity and recursive properties illustrated in §2, the dispersion relation takes the form

$$\cos(KL_n) = \frac{1}{2} \text{tr}(T_n(\omega)) \quad \Rightarrow \quad KL_n = \arccos\left(\frac{\text{tr}(T_n(\omega))}{2}\right), \quad (4.3)$$

where  $L_n$  is the length of the unit cell.

The pattern of pass and stop bands for this discrete mass-spring system is shown in figure 6 for various generalised Fibonacci tiling. In each case, the upper plot shows the band gaps of successive tilings  $\mathcal{F}_n$ , characterised as  $\omega$  such that  $|\text{tr}(T_n(\omega))| \leq 2$ . We can see how the spectrum becomes increasingly complex for increasing  $n$ . The middle plots of figure 6 show the super band gaps  $\mathcal{S}_N$ , which are computed by checking if  $\text{tr}(T_N(\omega))$  satisfies the growth condition from the theorems in §3. We see that the super band gaps agree with the pattern of spectral gaps observed in the top plot. By looking at the super band gaps  $\mathcal{S}_N$  for larger  $N$ , our theory is able to reveal some of the complex structure that emerges for  $\mathcal{F}_n$  with large  $n$  and shows that many of the smaller band gaps that are created are, in fact, super band gaps.

The lower plots in figure 6 show the super band gap estimator function  $H_2(\omega) = |\text{tr}(T_2(\omega))\text{tr}(T_3(\omega))|$  from [23]. We can see that the local maxima of  $H_2$  successfully predict the locations of the main few super band gaps, but that this approach is unable to reveal the complex pattern of super band gaps that emerges for higher-order Fibonacci tilings. This is one of the advantages of the new theory developed here, that higher resolution descriptions can be obtained by computing super band gaps  $\mathcal{S}_N$  for larger  $N$ , where required. We have not only developed a rigorously grounded theory for detecting for super band gaps, but our approach has greater resolution than was previously possible.

One notable feature of figure 6 is the occurrence of high-frequency super band gaps. That is, there appears to exist some  $\omega^*$  such that any  $\omega > \omega^*$  is in a super band gap. The origin for this phenomenon can be seen by inspecting the transfer matrices  $T^A$  and  $T^B$ , defined in (4.1). We have that

$$\text{tr}(T^X(\omega, m_X, k_X)) = 2 - \frac{m_X \omega^2}{k_X}, \quad (4.4)$$

so it is easy to see that if  $\omega > 2\sqrt{k_X/m_X}$  then  $\text{tr}(T^X) < -2$  so  $\omega$  is in a band gap of the material with label  $X$ . As a result, we have that if  $\omega > \max\{2\sqrt{k_A/m_A}, 2\sqrt{k_B/m_B}\}$  then  $\omega$  is in band gaps of both  $\mathcal{F}_0$  and  $\mathcal{F}_1$ , for any generalised Fibonacci tiling. However, this is not generally enough to guarantee that  $\omega$  is in a super band gap. For the discrete mass-spring system, the super band gap occurs due to the structure of the associated transfer matrices, which take a specific form when  $\omega$  is sufficiently large. This is made precise with the following result.

**Theorem 4.1.** Consider a discrete mass-spring system with behaviour governed by the equation (4.1) and fundamental cells designed according to a generalised Fibonacci substitution rule (2.1) with arbitrary  $m, l \geq 1$ . There exists some  $\omega^*$  such that if  $\omega > \omega^*$  then  $\omega$  is in the super band gap  $\mathcal{S}_0$ .

*Proof.* Suppose that  $\omega \rightarrow \infty$  while all the other parameters are kept constant. In this case, we have that

$$T^X = m_X \omega^2 \left( \begin{bmatrix} 0 & 0 \\ 1 & -k_X^{-1} \end{bmatrix} + O(\omega^{-2}) \right) \quad \text{as } \omega \rightarrow \infty. \quad (4.5)$$

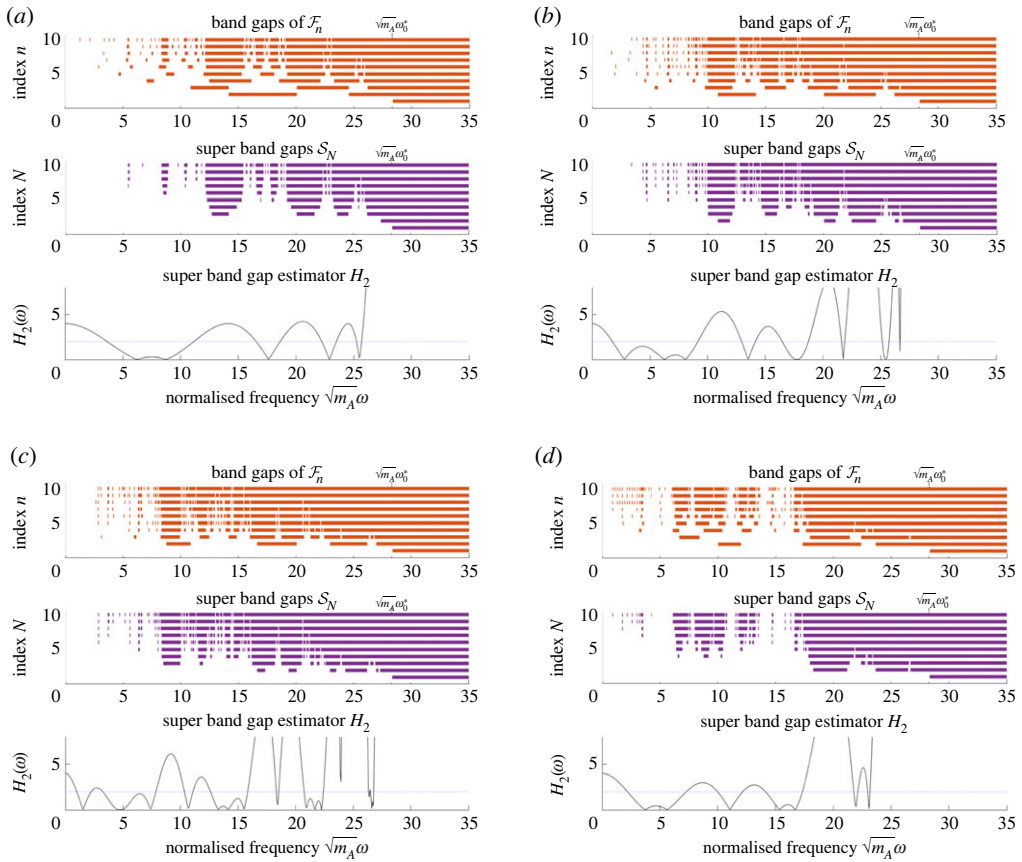


**Figure 6.** The band gaps and super band gaps of a discrete mass-spring system with spring constants varied according to generalised Fibonacci tilings  $\mathcal{F}_n$ . For each tiling, the top plot shows the band gaps for each successive Fibonacci tiling  $\mathcal{F}_n$ , the middle shows the super band gaps  $\mathcal{S}_n$ , as characterised by the corresponding theorem, and the bottom shows the super band gap estimator  $H_2$ , as used in previous works and defined in (2.12). We use the parameter values  $k_A = 2k_B = 200 \text{ N m}^{-1}$  and suppose that  $m_A = m_B$ . The normalised frequency  $\sqrt{m_A}\omega$  is shown on the horizontal axes and the value of the estimated threshold  $\omega_0^*$  from (4.8) is highlighted above. (a) Golden mean Fibonacci ( $m = 1, l = 1$ ), (b) silver mean Fibonacci ( $m = 2, l = 1$ ), (c) bronze mean Fibonacci ( $m = 3, l = 1$ ), (d) copper mean Fibonacci ( $m = 1, l = 2$ ).

Then, some straightforward algebra reveals that the transfer matrix of the generalised Fibonacci tiling  $\mathcal{F}_n$  satisfies

$$T_n = (m_A)^{mF_{n-2}}(m_B)^{lF_{n-1}}\omega^{2F_n} \left( \begin{bmatrix} 0 & 0 \\ \eta_1 & \eta_2 \end{bmatrix} + O(\omega^{-2}) \right) \quad \text{as } \omega \rightarrow \infty, \quad (4.6)$$

where  $\eta_1$  and  $\eta_2$  are non-zero constants and the generalised Fibonacci numbers  $F_n$  were defined in (2.3). Crucially, it holds that  $|\eta_2| \geq \max\{k_A, k_B\}^{-F_n}$ , so we can see that

$$|\text{tr}(T_n)| \geq \frac{(m_A)^{mF_{n-2}}(m_B)^{lF_{n-1}}\omega^{2F_n}}{\max\{k_A, k_B\}^{F_n}} \geq \left( \frac{\min\{m_A, m_B\}}{\max\{k_A, k_B\}} \omega^2 \right)^{F_n}. \quad (4.7)$$

As a result, we can see that if  $\omega$  is sufficiently large, then  $|\text{tr}(T_n)| > 2$  for all  $n$ , implying that  $\omega$  is in the super band gap  $\mathcal{S}_0$ . ■

While the bounds used to prove theorem 4.1 are quite loose in general, it is able to give some quantitative information on the high-frequency super band gap  $\mathcal{S}_1$ . In particular, from (4.7), it is clear that  $\min\{m_A, m_B\}\omega \geq 2 \max\{k_A, k_B\}$  is sufficient to guarantee that  $|\text{tr}(T_n)| \geq 2$  for all  $n$ . For

the parameter values considered in figure 6, this gives an upper estimate  $\omega_0^*$  for the normalised frequency of

$$\sqrt{m_A}\omega_0^* = \sqrt{800} \approx 28.28. \quad (4.8)$$

This value is indicated above the upper two plots in figure 6, where it can be seen to provide an accurate estimate for the lower limit of the super band gap  $\mathcal{S}_1$ . To characterise the lower limit of subsequent super band gaps, which can be observed to occur at successively lower frequencies, it is necessary to check the growth conditions derived in this work.

## (b) Axial waves in structured rods

The dispersive properties of two-phase quasi-periodic structured rods with unit cells generated by one-dimensional generalised Fibonacci sequences have been studied previously in [23], including experimentally in [20]. The lengths of the two segments  $A$  and  $B$  are indicated with  $l_A$  and  $l_B$ , respectively, while  $A_X$ ,  $E_X$  and  $\rho_X$  denote the cross-sectional area, Young's modulus and mass density per unit volume of the two adopted materials, respectively. This is sketched in figure 3*b*. For both elements, we define the displacement function and the axial force along the rod as  $u(z)$  and  $N(z) = EAu'(z)$ , respectively, where  $z$  is the coordinate describing the longitudinal axis (as depicted in figure 3). The governing equation of harmonic axial waves in each section is given by

$$\frac{d^2u}{dz^2}(z) + Q_X\omega^2u(z) = 0, \quad (4.9)$$

where  $Q_X = \rho_X/E_X$  corresponds to the reciprocal of the square of the speed of propagation of longitudinal waves in material  $X$ . The general solution of (4.9) is given by

$$u(z) = C_1^X \sin(\sqrt{Q_X}\omega z) + C_2^X \cos(\sqrt{Q_X}\omega z), \quad (4.10)$$

where  $C_1^X$  and  $C_2^X$  are integration constants, to be determined by the boundary conditions.

In order to obtain the dispersion diagram of the quasi-periodic rod, we express the state vector  $\mathbf{u}_{F_n} = [u_{F_n}, N_{F_n}]^T$  at the end of the Fibonacci unit cell as a function of the same vector  $\mathbf{u}_0 = [u_0, N_0]^T$  on the left-hand side

$$\mathbf{u}_{F_n} = T_n(\omega)\mathbf{u}_0, \quad (4.11)$$

where  $T_n(\omega)$  is a transfer matrix of the cell  $\mathcal{F}_n$ . This matrix is the result of the product  $T_n(\omega) = \prod_{p=1}^{F_n} T^X(\omega)$ , where  $T^X(\omega)$  ( $X \in \{A, B\}$ ) is the transfer matrix that relates quantities across a single element, given by

$$T^X(\omega) = \begin{bmatrix} \cos(\sqrt{Q_X}\omega l_X) & \frac{\sin(\sqrt{Q_X}\omega l_X)}{E_X A_X \sqrt{Q_X}} \\ -E_X A_X \omega \sqrt{Q_X} \sin(\sqrt{Q_X}\omega l_X) & \cos(\sqrt{Q_X}\omega l_X) \end{bmatrix}. \quad (4.12)$$

Once again, the matrices  $T_n(\omega)$  possess the important properties introduced in §2. As a consequence, if we impose the Floquet–Bloch condition  $\mathbf{u}_r = \mathbf{u}_l e^{iKL_n}$ , then the corresponding dispersion relation assumes a form identical to (4.3).

The pattern of pass and stop bands for this continuous system of structured rods is shown in figure 7 for several generalised Fibonacci tilings. As for the mass-spring system, we show the pattern of band gaps for successive tilings  $\mathcal{F}_n$  in the top subplot. Beneath this, we show the frequencies that are guaranteed to lie within super band gaps, thanks to the theorems from §3. We see good agreement between the super band gaps  $\mathcal{S}_N$  and the band gaps of  $\mathcal{F}_n$ . Once again, we see that whereas the estimator  $H_2$  is only able to predict the locations of the largest few super band gaps, our theory reveals a more intricate pattern of super band gaps.

One notable feature of the spectra in figure 7 is that they are symmetric and periodic. This is a consequence of the specific set-up we have chosen for these simulations, which has all the material parameters identical between  $A$  and  $B$  (i.e.  $E_A = E_B$ ,  $\rho_A = \rho_B$  and  $l_A = l_B$ ) and only the

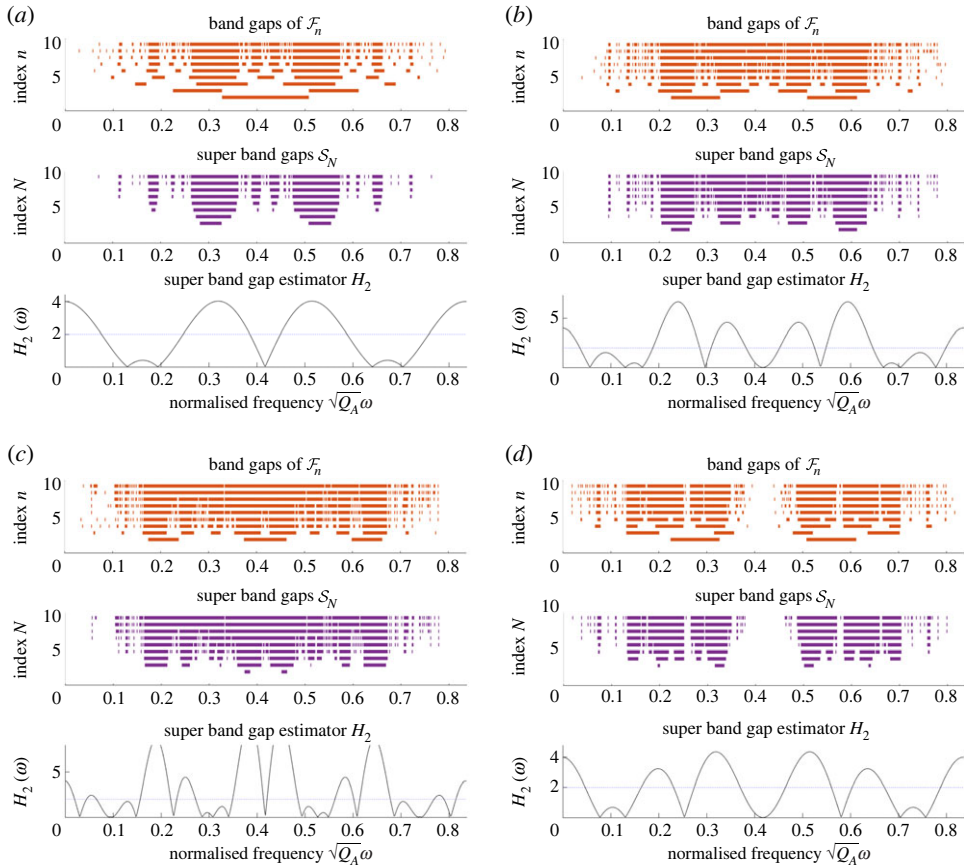


**Figure 7.** The band gaps and super band gaps of a system of structured rods with thickness varied according to generalised Fibonacci tilings  $\mathcal{F}_n$ . For each tiling, the top plot shows the band gaps for each successive Fibonacci tiling  $\mathcal{F}_n$ , the middle shows the super band gaps  $\mathcal{S}_N$ , as characterised by the corresponding theorem, and the bottom shows the super band gap estimator  $H_2$ , as used in previous works and defined in (2.12). We use the parameter values  $E_A = E_B = 3.3$  GPa,  $\rho_A = \rho_B = 1140$  kg m $^{-3}$ ,  $2A_A = A_B = 1.963 \times 10^{-3}$  m $^{-2}$ ,  $l_A = l_B = 0.07$  m. We plot the normalised frequency  $\sqrt{Q_A}\omega$  on the horizontal axes, noting that  $Q_A = Q_B$  in this case. (a) Golden mean Fibonacci ( $m = 1, l = 1$ ), (b) silver mean Fibonacci ( $m = 2, l = 1$ ), (c) bronze mean Fibonacci ( $m = 3, l = 1$ ), (d) copper mean Fibonacci ( $m = 1, l = 2$ ).

cross-sectional area modulated. As a result, the first three terms of the sequence of traces are given by

$$x_0(\omega) = x_1(\omega) = 2 \cos(\sqrt{Q_A}\omega l_A) \quad \text{and} \quad x_2(\omega) = 2 \cos^2(\sqrt{Q_A}\omega l_A) + \left(\frac{A_A}{A_B} + \frac{A_B}{A_A}\right) \sin^2(\sqrt{Q_A}\omega l_A). \quad (4.13)$$

It is easy to see that these functions are all periodic functions of  $\omega$ . This spectral symmetry and periodicity was explored through the symmetries of a coordinate transformation in [20], where they referred to this set-up as the ‘canonical configuration’.

### (c) Flexural waves in continuous beams with modulated supports

As a third prototype of one-dimensional Fibonacci-generated dynamical systems, we investigate the dispersive properties of flexural vibrations in a quasi-periodic multi-supported beam. In this case, we modulate the distances between the positions of the supports along the axis of the beam (figure 3c), choosing the lengths according to generalised Fibonacci tilings. The beam

is homogeneous, with bending stiffness denoted by  $EI$ , and the equation governing harmonic vibrations of the transverse displacement  $v(z)$  is

$$EI \frac{d^4 v}{dz^4} - \rho \omega^2 v = 0. \quad (4.14)$$

The solution of (4.14) can be expressed as  $v(z) = C \exp ikz$ , yielding the characteristic equation

$$(kr)^4 - P\omega^2 = 0, \quad (4.15)$$

where  $r$  is the radius of inertia of the cross section and  $P = \rho r^4 / EI$ . Equation (4.15) admits four solutions, namely

$$k_{1,2}(\omega) = \pm \frac{1}{r} \sqrt{\omega \sqrt{P}} \quad \text{and} \quad k_{3,4}(\omega) = \pm \frac{1}{r} \sqrt{-\omega \sqrt{P}}, \quad (4.16)$$

where the first index corresponds to the sign '+’.

We can now obtain the dispersion diagrams following the same procedure shown in the previous subsection for axial waves in structured rods. To do so, it is important to emphasise that the state of the multi-supported beam is determined by the rotation  $\phi(z)$  and its derivative  $\phi'(z)$  (or bending moment) at each supported point. This is because we assume that the beam is constrained to the support and there is no displacement there. This means that the fourth-order differential system (4.15) only has 2 d.f. This setting is well established and widely studied, see also [19]. The state vector on the right-hand side of the Fibonacci unit cell is then given by  $\mathbf{v}_{F_n} = [\phi_{F_n}, \phi'_{F_n}]^T$ , and it is related to  $\mathbf{v}_0 = [\phi_0, \phi'_0]^T$  through the relationship

$$\mathbf{v}_r = T_n(\omega) \mathbf{v}_l, \quad (4.17)$$

where, similarly to the previous cases,  $T_n(\omega) = \prod_{p=1}^{F_n} T^X(\omega)$  is the transfer matrix of the unit cell  $F_n$ . For this system, the transfer matrices  $T^X(\omega)$  ( $X \in \{A, B\}$ ) associated with each constituent unit are given in [19]

$$T^X(\omega) = \begin{bmatrix} \frac{\Psi_{bb}^X(\omega)}{\Psi_{ab}^X(\omega)} & \Psi_{ba}^X(\omega) - \frac{\Psi_{bb}^X(\omega)\Psi_{aa}^X(\omega)}{\Psi_{ab}^X(\omega)} \\ 1 & \frac{\Psi_{aa}^X(\omega)}{\Psi_{ab}^X(\omega)} \\ \frac{\Psi_{ab}^X(\omega)}{\Psi_{ab}^X(\omega)} & -\frac{\Psi_{aa}^X(\omega)}{\Psi_{ab}^X(\omega)} \end{bmatrix}, \quad (4.18)$$

where

$$\Psi_{aa}^X(\omega) = \frac{k_1(\omega) \cot(k_1(\omega)l_X) - k_3(\omega) \cot(k_3(\omega)l_X)}{k_3^2(\omega) - k_1^2(\omega)}, \quad \Psi_{bb}^X(\omega) = -\Psi_{aa}^X(\omega) \quad (4.19)$$

and

$$\Psi_{ab}^X(\omega) = \frac{k_1(\omega) \csc(k_1(\omega)l_X) - k_3(\omega) \csc(k_3(\omega)l_X)}{k_1^2(\omega) - k_3^2(\omega)}, \quad \Psi_{ba}^X(\omega) = -\Psi_{ab}^X(\omega), \quad (4.20)$$

and  $l_X$  ( $X \in \{A, B\}$ ) is the length of the simply supported beam  $A$  or  $B$ , representing the single element of our cells.

It is important to note that  $\Psi_{aa}^X(\omega)$  and  $\Psi_{ab}^X(\omega)$  both take only real values. This is because, although  $k_3(\omega)$  is always an imaginary number, each of  $k_3^2$ ,  $k_3 \cot(k_3 l_X)$  and  $k_3 \csc(k_3 l_X)$  are real. This means  $T^X$  always has real-valued entries. Further, we can algebraically check that  $T_n(\omega)$  satisfies the unimodularity condition and follows the recursive rule previously introduced. As a consequence, using the Floquet–Bloch condition  $\mathbf{v}_r = \mathbf{v}_l e^{iKL_n}$  into equation (4.17), we derive a dispersion relation similar to (4.3).

The pattern of pass and stop bands for this continuous system of multi-supported beams is shown in figure 8 for several generalised Fibonacci tilings. As with the previous examples, a complex pattern of band gaps emerges and the super band gap theory is able to accurately characterise this complex behaviour. In this case, the super band gap estimator  $H_2$ , that was developed in previous works (and is shown in the lower subplots), particularly struggles to reveal useful information about the detailed structure of the spectrum, demonstrating the value of our new theory.

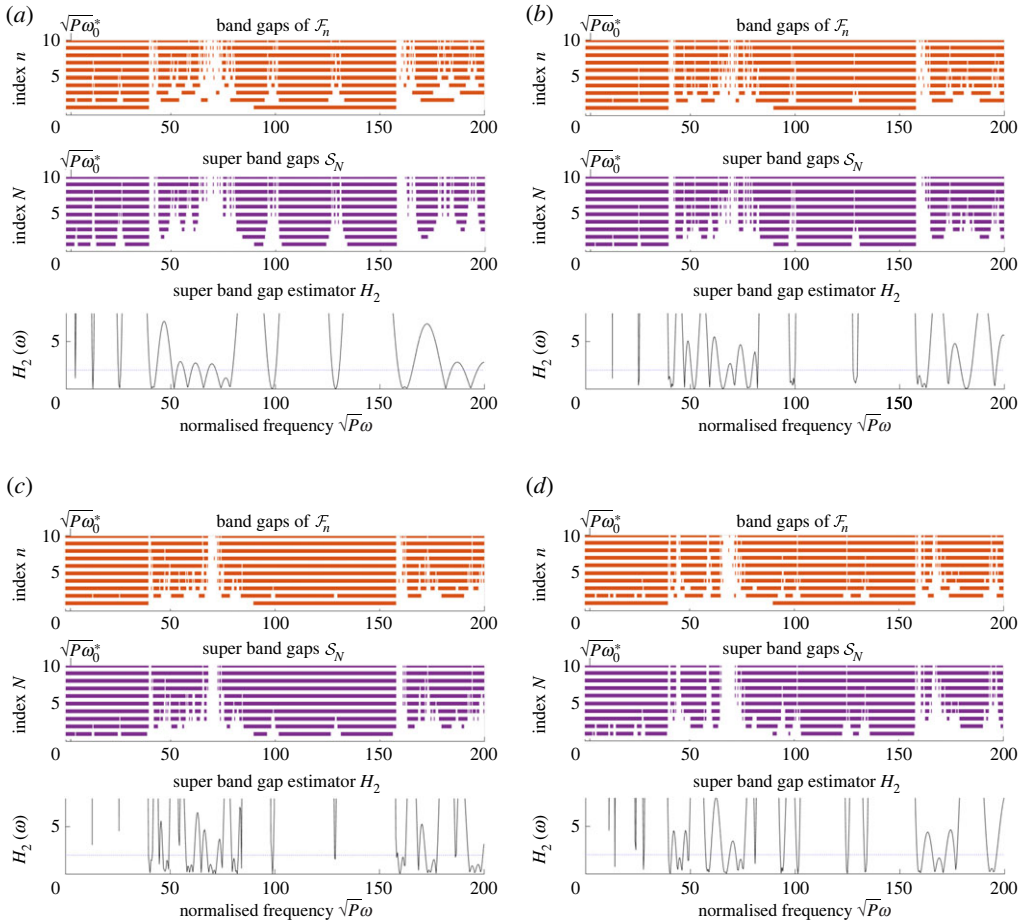


**Figure 8.** The band gaps and super band gaps of a continuous beam with supports modulated according to generalised Fibonacci tilings  $\mathcal{F}_n$ . For each tiling, the top plot shows the band gaps for each successive Fibonacci tiling  $\mathcal{F}_n$ , the middle shows the super band gaps  $\mathcal{S}_N$ , as characterised by the corresponding theorem, and the bottom shows the super band gap estimator  $H_2$ , as used in previous works and defined in (2.12). We use the distances  $4l_A = l_B = 0.1$  m between the supports and assume that all the material parameters are constant. In particular, we take  $r = 0.05$  m and plot the normalised frequency  $\sqrt{P}\omega$  on the horizontal axes. (a) Golden mean Fibonacci ( $m = 1, l = 1$ ), (b) silver mean Fibonacci ( $m = 2, l = 1$ ), (c) bronze mean Fibonacci ( $m = 3, l = 1$ ), (d) copper mean Fibonacci ( $m = 1, l = 2$ ).

A notable feature of the spectra in figure 8 is the occurrence of low-frequency super band gaps. As was the case for the high-frequency super band gaps that occurred in the mass-spring system, this can be understood by looking at the structure of the transfer matrices. We recall the function  $\text{sgn} : \mathbb{R} \rightarrow \{-1, 0, 1\}$  given by  $\text{sgn}(x) = x/|x|$  (and  $\text{sgn}(0) = 0$ ). Then, we introduce the sets of unimodular matrices  $\Sigma_+$  and  $\Sigma_-$  given by

$$\Sigma_+ := \{M \in \mathbb{R}^{2 \times 2} : \det(M) = 1, \text{sgn}(M_{11}) = \text{sgn}(M_{22}) = 1 \text{ and } \text{sgn}(M_{12}) = \text{sgn}(M_{21}) = -1\} \quad (4.21)$$

and

$$\Sigma_- := \{M \in \mathbb{R}^{2 \times 2} : -M \in \Sigma_+\}. \quad (4.22)$$

**Lemma 4.2.** Let  $T^X(\omega)$  be the transfer matrix of the multi-supported beam, as defined in (4.18). There exists some  $\omega^{*,X} > 0$  such that  $T^X(\omega) \in \Sigma_-$  for all  $0 < \omega < \omega^{*,X}$ . Further, it holds that

$$T^X(\omega) = \begin{bmatrix} -2 & l_X/2 \\ \frac{6}{l_X} & -2 \end{bmatrix} + O(\omega), \quad \text{as } \omega \rightarrow 0.$$

*Proof.* Suppose that  $\omega \rightarrow \infty$  while all the other parameters are kept constant. Recalling (4.16), we see that  $k_i = O(\omega^{1/2})$  and, using the Taylor series for cot and csc,

$$k_1(\omega) \cot(k_1(\omega)l_X) = \frac{1}{l_X} - \frac{k_1^2 l_X}{3} + O(\omega^2) \quad \text{and} \quad k_1(\omega) \csc(k_1(\omega)l_X) = \frac{1}{l_X} - \frac{k_1^2 l_X}{6} + O(\omega^2), \quad (4.23)$$

as  $\omega \rightarrow 0$ . Substituting these expressions into (4.19) and (4.20) gives us that

$$\Psi_{aa}^X = \frac{l_X}{3} + O(\omega) \quad \text{and} \quad \Psi_{ab}^X = \frac{l_X}{6} + O(\omega), \quad (4.24)$$

as  $\omega \rightarrow 0$ . Substituting this into the expression (4.18), we obtain the leading-order expression for  $T^X$ . Since the leading-order matrix is in  $\Sigma_-$ ,  $T^X$  will be in  $\Sigma_-$  provided  $\omega$  is sufficiently small. ■

**Lemma 4.3.** Suppose that  $0 < \omega < \min\{\omega^{*,A}, \omega^{*,B}\}$  and let  $T_n$  be the transfer matrix associated with a multi-supported beam with fundamental cell designed according to a generalised Fibonacci substitution rule (2.1) with arbitrary  $m, l \geq 1$ .  $T_n \in \Sigma_-$  if  $F_n$  is odd and  $T_n \in \Sigma_+$  if  $F_n$  is even.

*Proof.* From lemma 4.2, we have that both  $T^A \in \Sigma_-$  and  $T^B \in \Sigma_-$ . It is straightforward to verify that

$$\Sigma_- \otimes \Sigma_- = \Sigma_+ \otimes \Sigma_+ = \Sigma_+ \quad \text{and} \quad \Sigma_- \otimes \Sigma_+ = \Sigma_+ \otimes \Sigma_- = \Sigma_-. \quad (4.25)$$

Then, if  $F_n$  is even,  $T_n$  is the product of an even number of matrices from  $\Sigma_-$ , meaning it is the product of  $F_n/2$  matrices from  $\Sigma_+$ , so  $T_n \in \Sigma_-$ . Conversely, if  $F_n$  is odd, then  $T_n$  may be written as the product of  $F_n - 1$  matrices in  $\Sigma_-$  and another matrix in  $\Sigma_-$ . Since  $F_n - 1$  is even, the first of these two terms is in  $\Sigma_+$ , meaning  $T_n \in \Sigma_+ \otimes \Sigma_- = \Sigma_-$ . ■

We are now in a position to prove an analogous result to theorem 4.1, which demonstrates the existence of low-frequency super band gaps for the multi-supported beam (based on the structure of the transfer matrices and without needing to check the growth conditions). From lemma 4.2, we can see that  $\omega$  will be in a band gap of both  $\mathcal{F}_0$  and  $\mathcal{F}_1$  if it is sufficiently small. However, as was the case for the discrete system, we must take advantage of the specific structure of the transfer matrices in this regime to prove a result.

**Theorem 4.4.** Consider a multi-supported beam with behaviour governed by the equation (4.17) and fundamental cells designed according to a generalised Fibonacci substitution rule (2.1) with arbitrary  $m, l \geq 1$ . There exists some  $\omega^* > 0$  such that if  $0 < \omega < \omega^*$  then  $\omega$  is in the super band gap  $\mathcal{S}_0$ .

*Proof.* The key to our argument is proving that

$$|(T_n)_{11}| \geq 2^{F_n} \quad \text{and} \quad |(T_n)_{22}| \geq 2^{F_n}. \quad (4.26)$$

We first consider the golden mean Fibonacci case, where  $m = l = 1$ , and proceed by induction. From lemma 4.2, we can see that (4.26) holds for both  $T_0 = T^B$  and  $T_1 = T^A$ . Then, for an arbitrary  $n \geq 1$ , it holds for the golden mean Fibonacci tiling that

$$(T_{n+1})_{11} = (T_{n-1})_{11}(T_n)_{11} + (T_{n-1})_{12}(T_n)_{21} \quad (4.27)$$

and

$$(T_{n+1})_{22} = (T_{n-1})_{22}(T_n)_{22} + (T_{n-1})_{21}(T_n)_{12}. \quad (4.28)$$

Lemma 4.3 implies that  $T_{n-1}, T_n \in \Sigma_+ \cup \Sigma_-$ , hence it holds that  $\text{sgn}((T_{n-1})_{11}(T_n)_{11}) = \text{sgn}((T_{n-1})_{12}(T_n)_{21})$  and similarly  $\text{sgn}((T_{n-1})_{22}(T_n)_{22}) = \text{sgn}((T_{n-1})_{21}(T_n)_{12})$ . As a result, we find

that

$$|(T_{n+1})_{11}| > |(T_{n-1})_{11}(T_n)_{11}| \geq 2^{F_{n-1}+F_n} = 2^{F_{n+1}} \quad (4.29)$$

and

$$|(T_{n+1})_{22}| > |(T_{n-1})_{22}(T_n)_{22}| \geq 2^{F_{n-1}+F_n} = 2^{F_{n+1}}. \quad (4.30)$$

Then, we can proceed by induction to conclude that (4.26) holds for all  $n$ , for the golden mean Fibonacci case. For arbitrary  $m, l \geq 1$ , we can use a similar argument, where the key step is to realise that the terms in the equivalent expansions to (4.27) and (4.28) all have the same sign. As a result, we have the desired bounds

$$|(T_{n+1})_{11}| > |(T_{n-1})_{11}^l (T_n)_{11}^m| \geq 2^{lF_{n-1}+mF_n} = 2^{F_{n+1}} \quad (4.31)$$

and

$$|(T_{n+1})_{22}| > |(T_{n-1})_{22}^l (T_n)_{22}^m| \geq 2^{lF_{n-1}+mF_n} = 2^{F_{n+1}}, \quad (4.32)$$

meaning (4.26) holds for any generalised Fibonacci tiling.

Finally, thanks to lemma 4.3, we know that  $(T_n)_{11}$  and  $(T_n)_{22}$  must have the same sign. Hence, it follows from (4.26) that  $|\text{tr}(T_n)| \geq 2^{F_{n+1}} > 2$ , so  $\omega$  must be in a band gap for all  $n$ . ■

Theorem 4.4 shows that the multi-supported beam system necessarily inherits the low-frequency band gap from its constituent elements (in the form of a super band gap). It can be used to provide a crude estimate of the upper limit  $\omega_0^*$  (analogous to (4.8) for the mass-spring system). In this case, however, the less straightforward form of the transfer matrices makes an explicit and tight bound difficult to come by. One simple approach is to notice that the arguments in theorem 4.4 rely on the property that the transfer matrices  $T^A$  and  $T^B$  necessarily belong to either  $\Sigma_+$  or  $\Sigma_-$  when the frequency is sufficiently low. As a result, a simple numerical estimate for  $\omega^*$  can be calculated by finding the smallest frequency  $\omega$  for which at least one of  $T^A$  or  $T^B$  does not belong to  $\Sigma_+ \cup \Sigma_-$ . This value is shown in figure 8 (above the two upper plots), where it is clear that it provides only a very loose bound on the low-frequency super band gap. This demonstrates the value of the growth condition approach for identifying super band gaps, which provides a much tighter bound for this example and does not rely on decoding the specific properties of the system (and its associated transfer matrices).

## 5. Periodic approximants

The aim of this final section is use our theory of super band gaps to predict the dynamical properties of finite-sized sections of quasicrystalline structures, as would be realised in experiments and applications. To this end, we take a piece of a one-dimensional Fibonacci quasicrystal and compare its transmission coefficient with the stop and pass band diagrams obtained by applying the Floquet–Bloch theory to the infinitely periodic systems generated by consecutive Fibonacci cells  $\mathcal{F}_n$ . We will present results for the case of a structured rod, as studied in §4b, but it is reasonable to expect similar behaviour for the other physical systems also.

The Fibonacci quasicrystal we take, as a demonstrative example, is a finite rod formed by joining together golden mean cells  $\mathcal{F}_0, \mathcal{F}_1$  all the way up to  $\mathcal{F}_6$ . This gives a structure composed of 32 different phases  $A$  and  $B$ , as depicted in figure 9. The self-similar nature of the Fibonacci-generated pattern (as illustrated by the annotations in figure 1, for example) means that this system will contain many (non-periodic) repetitions of the smaller unit cells  $\mathcal{F}_2 = AB, \mathcal{F}_3 = ABA, \mathcal{F}_4 = ABAAB$  and so on. As a result, it is reasonable to expect that its transmission properties can be well approximated by the super band gaps arising from these smaller unit cells. Considering axial vibrations propagating in this system, the global transfer matrix is defined as  $T_C(\omega) = \Pi_{n=1}^6 T_n(\omega)$ , where  $T_n(\omega)$  are the matrices associated with the cells  $\mathcal{F}_n$  that were introduced in

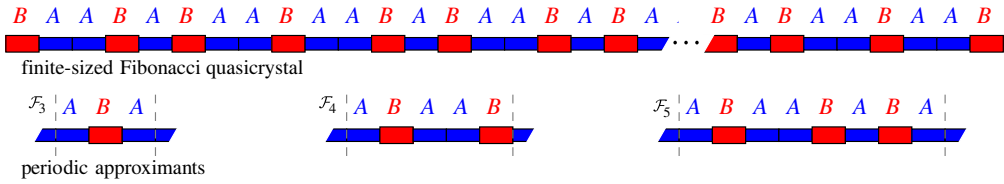


**Figure 9.** Our results show that the main spectral gaps of a finite-sized piece of a Fibonacci quasicrystal can be faithfully predicted by periodic approximants. We compare the transmission coefficient of a quasi-periodic structured rod of finite length (shown in the top row) with the Bloch spectra of periodic approximants (periodic approximants with unit cells  $\mathcal{F}_3$ ,  $\mathcal{F}_4$  and  $\mathcal{F}_5$  are shown in the bottom row). The numerical results are shown in figures 10 and 11.

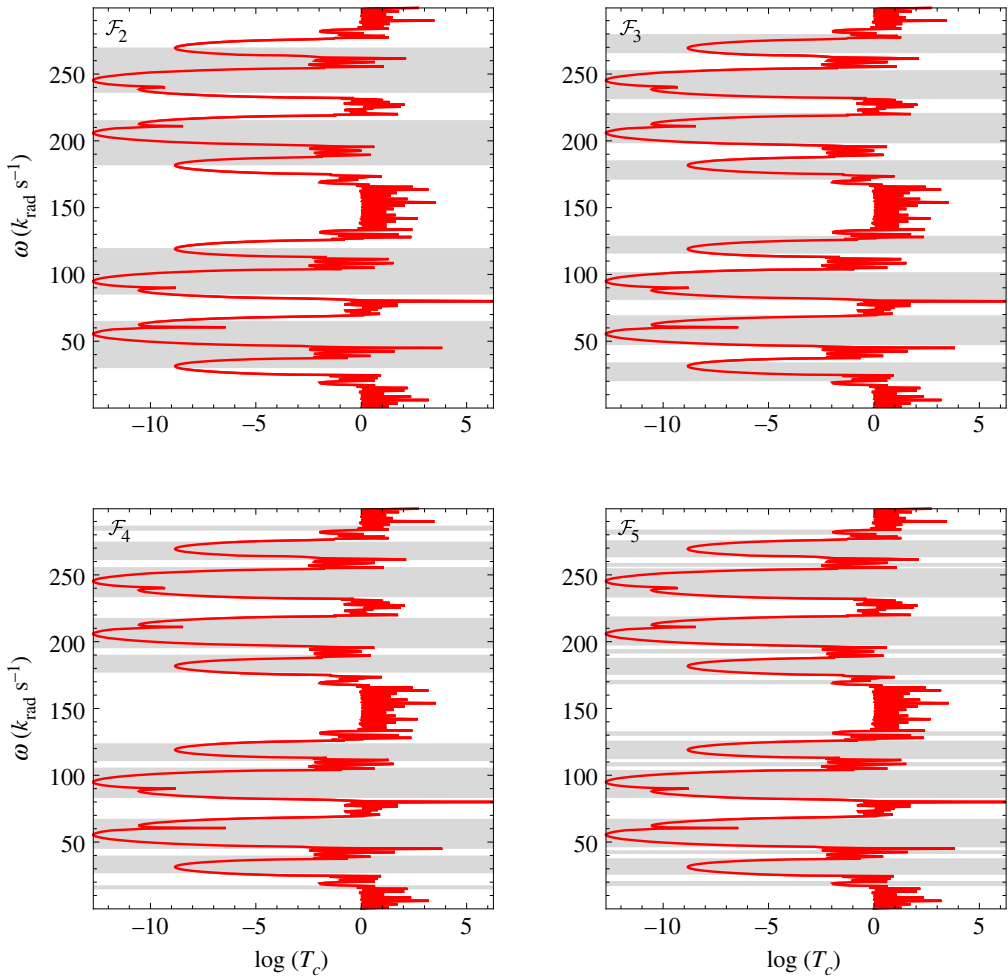


**Figure 10.** Transmission coefficient for a finite-sized piece quasicrystalline rod composed of golden mean cells  $\mathcal{F}_0$  to  $\mathcal{F}_6$  (red line) compared with the super band gaps of infinite structures generated according to  $\mathcal{F}_2$ ,  $\mathcal{F}_3$ ,  $\mathcal{F}_4$  and  $\mathcal{F}_5$  (grey shaded areas). We use the parameter values  $E_A = E_B = 3.3 \text{ GPa}$ ,  $\rho_A = \rho_B = 1140 \text{ kg m}^{-3}$ ,  $4A_A = A_B = 1.963 \times 10^{-3} \text{ m}^2$ ,  $l_A = 2l_B = 0.07 \text{ m}$ . The frequency range is shown on the vertical axis and the logarithm of the transmission coefficient  $\log(T_c)$  is plotted on the horizontal axis.

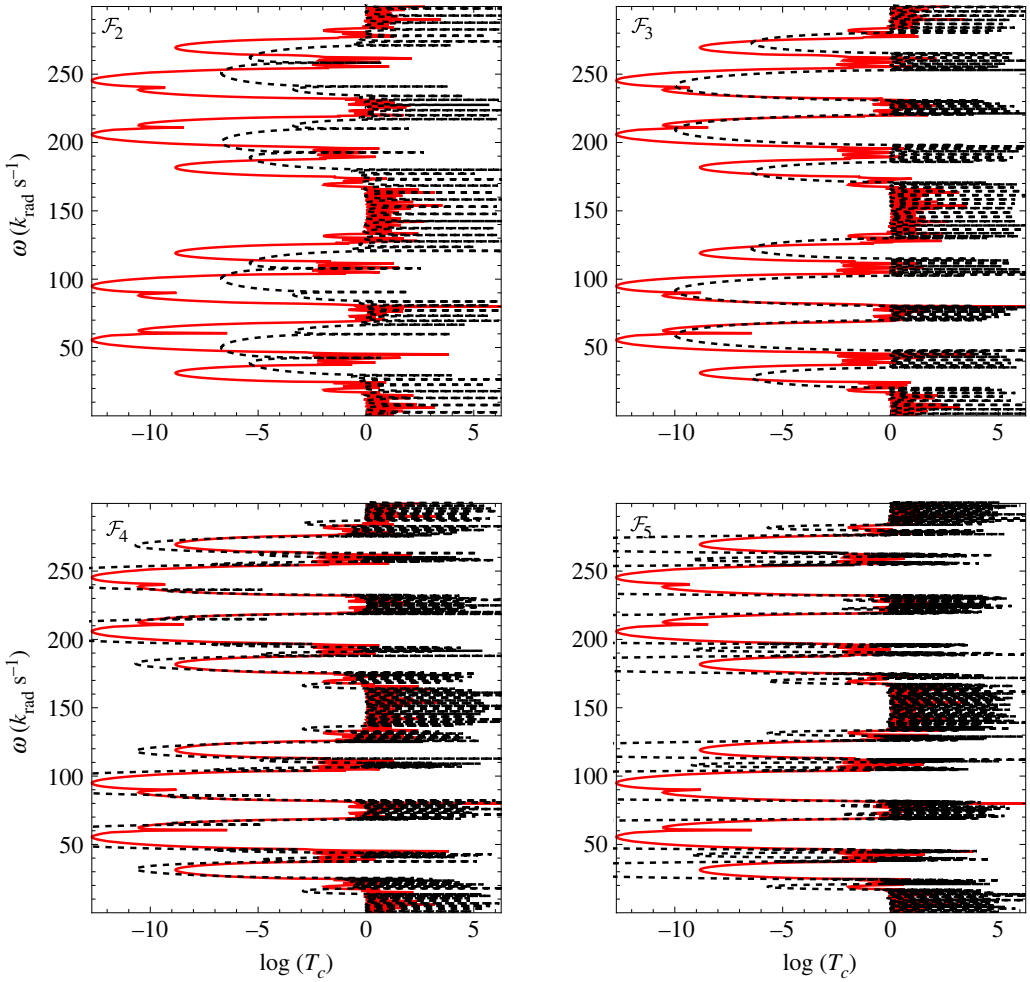


**Figure 11.** Transmission coefficients for a finite-sized piece of a quasicrystalline rod composed of golden mean cells  $\mathcal{F}_0$  to  $\mathcal{F}_6$  (red line) and for a finite-sized pieces of periodic samples consisting of seven repetitions of the unit cells  $\mathcal{F}_2$ ,  $\mathcal{F}_3$ ,  $\mathcal{F}_4$  and  $\mathcal{F}_5$  (black dashed lines). We use the parameter values  $E_A = E_B = 3.3$  GPa,  $\rho_A = \rho_B = 1140$  kg m $^{-3}$ ,  $4A_A = A_B = 1.963 \times 10^{-3}$  m $^2$ ,  $l_A = 2l_B = 0.07$  m. The frequency range is shown on the vertical axis and the logarithm of the transmission coefficient  $T_c$  is plotted on the horizontal axis.

§4b. According to the method adopted in [20], it can be shown that the transmission coefficient for a finite quasicrystalline sample is given by

$$T_c(\omega) = \frac{u_l}{u_r} = \frac{1}{T_{G22}(\omega)}, \quad (5.1)$$

where  $T_{G22}$  is the lower-right entry of the  $2 \times 2$  square matrix  $T_G$ .

In figure 10, the transmission coefficient  $T_c(\omega)$  for the finite quasicrystalline rod is plotted using a logarithmic scale. In each of the four plots, this is compared with the super band gaps exhibited by  $\mathcal{F}_2, \mathcal{F}_3, \mathcal{F}_4$  and  $\mathcal{F}_5$  (i.e. the sets  $\mathcal{S}_2, \mathcal{S}_3, \mathcal{S}_4$  and  $\mathcal{S}_5$ , to use the notation from §3). For these numerical computations we adopted a set-up that leads to a periodic and symmetric spectrum, as mentioned in §4b and referred to as the ‘canonical configuration’ in [20]. Therefore, the results reported for one period describe the dispersion properties for the whole range of real frequencies. We observe that, as the order of the Fibonacci unit cells increases, the super band gaps given by the periodic rods (denoted by the grey shaded areas) closely match the frequency intervals where

the transmission coefficient is small. For the unit cell  $\mathcal{F}_5$ , the drops in the transmission coefficient and the super band gaps are almost indistinguishable by eye (for this reason, there is no value in considering the super band gaps for any larger unit cells). This shows that, for this example, the super band gaps corresponding to a periodic infinite rod with a relatively small fundamental cell provide a good approximation for the spectrum of finite non-periodic quasicrystalline structures.

In figure 11, the same transmission coefficient  $T_c(\omega)$  is plotted, but this time, we compare it with the transmission spectrum of a periodic approximant. In this case, the transmission coefficient for a finite-sized piece of periodic material is shown with a dotted line, again for the simple golden mean Fibonacci tilings. The finite pieces of periodic material are composed of  $\mathcal{N}$  elementary cells  $\mathcal{F}_2, \mathcal{F}_3, \mathcal{F}_4$  and  $\mathcal{F}_5$ . The global transfer matrix for these finite periodic rods is then defined as  $T_G(\omega) = T_n^{\mathcal{N}}(\omega)$ . The results reported in figure 11 are obtained assuming  $\mathcal{N} = 7$ , meaning that the number of elements within each of the periodic samples is  $\tilde{F}_n = 7F_n$ , where  $F_n$  is the Fibonacci golden number corresponding to the phases contained in  $\mathcal{F}_n$  (i.e. for  $\mathcal{F}_2$  finite rod,  $F_2 = 2$  and  $\tilde{F}_2 = 14$ ). The choice  $\mathcal{N} = 7$  is made so that the decay of the solution within the band gaps is sufficiently clear. The transmission coefficient would drop more if a larger number of unit cells was used (although the nature of exponential decay means that this effect diminishes with larger  $\mathcal{N} = 7$ ). Even when the periodic approximant has a small unit cell (so the approximation is relatively crude), such as for example in the case of  $\mathcal{F}_3$  ( $F_3 = 3$  and  $\tilde{F}_3 = 21$ ), the main spectral gaps are accurately predicted. This is naturally explained by our theory for super band gaps, which provides sufficient conditions for intervals of frequency to always be in spectral gaps, for any sufficiently large unit cell drawn from the sequence generated by the generalised Fibonacci tiling rules.

## 6. Conclusion

We have developed a novel mathematical theory for characterizing super band gaps in periodic structures generated by generalised Fibonacci tilings. This illuminates the mechanism through which structural self similarity creates identifiable features in the otherwise complex spectra of quasi-periodic systems. Our results provide some justification for the use of periodic approximants (supercells) to predict the spectra of generalised Fibonacci tilings, as we have proved that the properties of a given element in this sequence of tilings can be used to predict spectral characteristics (in particular, some of the main band gaps) of all subsequent elements in the sequence. We have examined this by considering a large quasicrystalline material, which is made from several different Fibonacci tiles, and shown that the frequency ranges where its transmission coefficient drops are in close correspondence with the super band gaps predicted by periodic approximants (even with relatively small unit cells).

This work provides a concise and computationally efficient way to detect the main spectral features of quasicrystalline materials generated by generalised Fibonacci tilings. This is crucial if such materials are to be used in wave control applications, which has been the subject of several recent studies. For example, Fibonacci tilings have been used as the basis for designing symmetry-induced waveguides [29] and laminar materials that exhibit negative refraction [35]. Similar studies have also been conducted for other quasicrystals, such as variants of the Harper model [36–38] and arbitrary cut-and-project quasicrystals [39] (of which Fibonacci tilings are a subset). Understanding a material's spectral gaps is essential for the design of any such device, and the results in this work (which could be generalised to other quasicrystalline materials generated by tiling rules [40,41]) provide a first step for doing so.

**Data accessibility.** This article has no additional data.

**Declaration of AI use.** We have not used AI-assisted technologies in creating this article.

**Authors' contributions.** B.D.: conceptualisation, formal analysis, investigation, methodology, software, visualisation, writing—original draft, writing—review and editing; L.M.: conceptualisation, formal analysis, investigation, methodology, software, visualisation, writing—original draft, writing—review and editing.

Both authors gave final approval for publication and agreed to be held accountable for the work performed therein.

**Conflict of interest declaration.** We declare we have no competing interests.

**Funding.** The work of B.D. was supported by a fellowship from the Engineering and Physical Sciences Research Council (EPSRC) with grant no. EP/X027422/1. L.M. thanks the support of Cardiff University. The software developed for this study is available at <https://doi.org/10.5281/zenodo.7602934> [42].

## References

1. Kadic M, Milton GW, van Hecke M, Wegener M. 2019 3D metamaterials. *Nature Rev. Phys.* **1**, 198–210. (doi:10.1038/s42254-018-0018-y)
2. Colbrook MJ, Roman B, Hansen AC. 2019 How to compute spectra with error control. *Phys. Rev. Lett.* **122**, 250201. (doi:10.1103/PhysRevLett.122.250201)
3. Hege P, Moscolari M, Teufel S. 2022 Finding spectral gaps in quasicrystals. *Phys. Rev. B* **106**, 155140. (doi:10.1103/PhysRevB.106.155140)
4. Avila A, Jitomirskaya S. 2009 The ten martini problem. *Ann. Math.* **170**, 303–342. (doi:10.4007/annals.2009.170.303)
5. Eliasson LH. 1992 Floquet solutions for the 1-dimensional quasi-periodic Schrödinger equation. *Commun. Math. Phys.* **146**, 447–482. (doi:10.1007/BF02097013)
6. Gumbs G, Ali MK. 1988 Dynamical maps, Cantor spectra, and localization for Fibonacci and related quasiperiodic lattices. *Phys. Rev. Lett.* **60**, 1081. (doi:10.1103/PhysRevLett.60.1081)
7. Kohmoto M, Oono Y. 1984 Cantor spectrum for an almost periodic Schrödinger equation and a dynamical map. *Phys. Lett. A* **102**, 145–148. (doi:10.1016/0375-9601(84)90928-9)
8. Jitomirskaya SY. 1999 Metal-insulator transition for the almost Mathieu operator. *Ann. Math.* **150**, 1159–1175. (doi:10.2307/121066)
9. Surace S. 1990 The Schrödinger equation with a quasi-periodic potential. *Trans. Am. Math. Soc.* **320**, 321–370. (doi:10.1090/S0002-9947-1990-0998358-6)
10. Bouchitté G, Guenneau S, Zolla F. 2010 Homogenization of dielectric photonic quasi crystals. *Multiscale Model. Simul.* **8**, 1862–1881. (doi:10.1137/090770333)
11. Wellander N, Guenneau S, Cherkasov E. 2018 Two-scale cut-and-projection convergence; homogenization of quasiperiodic structures. *Math. Methods Appl. Sci.* **41**, 1101–1106. (doi:10.1002/mma.4345)
12. Amenoagbadji P, Fliss S, Joly P. 2023 Wave propagation in one-dimensional quasiperiodic media. (<http://arxiv.org/abs/2301.01159>)
13. Rodriguez AW, McCauley AP, Avniel Y, Johnson SG. 2008 Computation and visualization of photonic quasicrystal spectra via Bloch's theorem. *Phys. Rev. B* **77**, 104201. (doi:10.1103/PhysRevB.77.104201)
14. Chan Y, Chan CT, Liu Z. 1998 Photonic band gaps in two dimensional photonic quasicrystals. *Phys. Rev. Lett.* **80**, 956. (doi:10.1103/PhysRevLett.80.956)
15. Florescu M, Torquato S, Steinhardt PJ. 2009 Complete band gaps in two-dimensional photonic quasicrystals. *Phys. Rev. B* **80**, 155112. (doi:10.1103/PhysRevB.80.155112)
16. Hamilton JK, Camacho M, Boix R, Hooper IR, Lawrence CR. 2021 Effective-periodicity effects in Fibonacci slot arrays. *Phys. Rev. B* **104**, L241412. (doi:10.1103/PhysRevB.104.L241412)
17. Kolář M. 1993 New class of one-dimensional quasicrystals. *Phys. Rev. B* **47**, 5489. (doi:10.1103/PhysRevB.47.5489)
18. Dal Negro L, Feng NN. 2007 Spectral gaps and mode localization in Fibonacci chains of metal nanoparticles. *Opt. Express* **15**, 14 396–14 403. (doi:10.1364/OE.15.014396)
19. Gei M. 2010 Wave propagation in quasiperiodic structures: stop/pass band distribution and prestress effect. *Int. J. Solids Struct.* **517**, 3067–3075. (doi:10.1016/j.ijsolstr.2010.07.008)
20. Gei M, Chen Z, Bosi F, Morini L. 2020 Phononic canonical quasicrystalline waveguides. *Appl. Phys. Lett.* **116**, 241903. (doi:10.1063/5.0013528)
21. Hiramoto H, Kohmoto M. 1989 New localization in a quasiperiodic system. *Phys. Rev. Lett.* **62**, 2714. (doi:10.1103/PhysRevLett.62.2714)
22. Kraus YE, Zilberberg O. 2012 Topological equivalence between the Fibonacci quasicrystal and the Harper model. *Phys. Rev. Lett.* **109**, 116404. (doi:10.1103/PhysRevLett.109.116404)
23. Morini L, Gei M. 2018 Waves in one-dimensional quasicrystalline structures: dynamical trace mapping, scaling and self-similarity of the spectrum. *J. Mech. Phys. Solids* **119**, 83–103. (doi:10.1016/j.jmps.2018.06.007)
24. Moustaj A, Röntgen M, Morfonios CV, Schmelcher P, Smith CM. 2023 Spectral properties of two coupled Fibonacci chains. *New J. Phys.* **25**, 093019. (doi:10.1088/1367-2630/acf0e0)

25. Kolář M, Ali MK. 1989 Generalized Fibonacci superlattices, dynamical trace maps, and magnetic excitations. *Phys. Rev. B* **39**, 426. (doi:10.1103/PhysRevB.39.426)
26. Kolář M, Nori F. 1990 Trace maps of general substitutional sequences. *Phys. Rev. B* **42**, 1062. (doi:10.1103/PhysRevB.42.1062)
27. Kolář M, Ali MK. 1990 One-dimensional generalized Fibonacci tilings. *Phys. Rev. B* **41**, 7108. (doi:10.1103/PhysRevB.41.7108)
28. Kohmoto M, Kadanoff LP, Tang C. 1983 Localization problem in one dimension: mapping and escape. *Phys. Rev. Lett.* **50**, 1870. (doi:10.1103/PhysRevLett.50.1870)
29. Davies B, Craster RV. 2022 Symmetry-induced quasicrystalline waveguides. *Wave Motion* **115**, 103068. (doi:10.1016/j.wavemoti.2022.103068)
30. Bender CM, Orszag SA. 1999 *Advanced mathematical methods for scientists and engineers I: Asymptotic methods and perturbation theory*. New York, NY: Springer Science & Business Media.
31. Horn RA, Johnson CR. 2012 *Matrix analysis*, 2nd edn. Cambridge, UK: Cambridge University Press.
32. Kolář M, Ali MK. 1989 Attractors of some volume-nonpreserving Fibonacci trace maps. *Phys. Rev. A* **39**, 6538. (doi:10.1103/PhysRevA.39.6538)
33. Lázaró M, Niemczynowicz A, Siemaszko A, García-Raffi LM. 2022 Elastodynamical properties of Sturmian structured media. *J. Sound Vib.* **517**, 116539. (doi:10.1016/j.jsv.2021.116539)
34. Rui X, Wang G, Zhang J. 2019 *Transfer matrix method for multibody systems: theory and applications*. Singapore: John Wiley & Sons.
35. Morini L, Eyzat Y, Gei M. 2019 Negative refraction in quasicrystalline multilayered metamaterials. *J. Mech. Phys. Solids* **124**, 282–298. (doi:10.1016/j.jmps.2018.10.016)
36. Apigo DJ, Qian K, Prodan C, Prodan E. 2018 Topological edge modes by smart patterning. *Phys. Rev. Mater.* **2**, 124203. (doi:10.1103/PhysRevMaterials.2.124203)
37. Martí-Sabaté M, Torrent D. 2021 Edge modes for flexural waves in quasi-periodic linear arrays of scatterers. *APL Mater.* **9**, 081107. (doi:10.1063/5.0059097)
38. Pal RK, Rosa MIN, Ruzzene M. 2019 Topological bands and localized vibration modes in quasiperiodic beams. *New J. Phys.* **21**, 093017. (doi:10.1088/1367-2630/ab3cd7)
39. Davies B, Chaplain GJ, Starkey TA, Craster RV. 2023 Graded quasiperiodic metamaterials perform fractal rainbow trapping. *Phys. Rev. Lett.* **131**, 177001. (doi:10.1103/PhysRevLett.131.177001)
40. Grünbaum B, Shephard GC. 1987 *Tilings and patterns*. New York, NY: W.H. Freeman.
41. Maciá E. 2014 On the nature of electronic wave functions in one-dimensional self-similar and quasiperiodic systems. *ISRN Condens. Matter Phys.* **2014**, 165943.
42. Davies B, Morini L. 2024 Super band gaps and periodic approximants of generalized Fibonacci tilings. *Zenodo*. (doi:10.5281/zenodo.7602934)